CHARACTERIZATION OF THE BONE MARROW NICHE IN ACUTE MYELOID LEUKEMIA PATIENTS

CHARACTERIZATION OF THE BONE MARROW NICHE IN ACUTE MYELOID LEUKEMIA PATIENTS

By CHARISA HENLY, B.Sc. (Honours)

A Thesis Submitted to the School of Graduate Studies in Partial Fulfillment of the Requirements for the Degree Master of Science

McMaster University

Descriptive Note

McMaster University MASTER OF SCIENCE (2022) Hamilton, Ontario (Biochemistry and Biomedical Science)

TITLE:	Characterization of the bone marrow niche in Acute Myeloid Leukemia patients
AUTHOR:	Charisa Henly, B.Sc. (Honours)
SUPERVISOR:	Dr. Mick Bhatia
NUMBER OF PAGES:	xii, 77

Abstract

The bone marrow (BM) microenvironment (the niche) plays a critical role in regulating normal hematopoietic process and is dysregulated in bone and marrow-related malignancies such as Acute Myeloid Leukemia (AML). AML is an aggressive blood cancer affecting the myeloid lineage of the hematopoietic hierarchy, and occurs in mostly individuals of older age. The goal in recent years has been to prolong the survival of these elderly patients, who show morbidity and early induction mortality in the face of intensive treatments. Disease relapse also poses a major hurdle to overcome following the supposed eradication of the leukemic disease, as current disease monitoring strategies used to detect minimal residual disease (MRD) are insufficient and may vary between patients. Many turn to look at the hematopoietic niche for the development of non-cell autonomous AML therapies in the hopes of more targeted and tolerable therapies; however, these strategies focus solely on the elimination of leukemic cells, and remain ignorant to the deterioration of the niche stemming from the disease. As yet, studies on niche cells, including mesenchymal stem cells and their progenies, are riddled with discrepancies and remain challenging to perform as methods used in the field to investigate mesenchymal populations rely primarily on *ex vivo* assays which are subject to extraneous factors that can lead to biased interpretation. Here, we used an *in vitro* mesenchymal CFU assay to interrogate the BM niche of AML patients and identify aberrations to the diseased niche throughout progression of the leukemic disease. Our experimental findings showed that while BM adipocyte and osteoblast populations appeared to be equally impaired in AML patients, the reduction in adipogenesis capacity of BM mesenchymal cells seemed to be unique in relapsed patients. We further identified a novel adipogenesis-inducing molecule, Isoginkgetin, that can successfully correct this deficiency in AML BM-MSCs and promote BM adipogenesis *in vivo.*

Acknowledgments

I would like to thank Dr. Mick Bhatia for your guidance, for being the biggest driving force behind my pursuit of scientific research, and for having given me a chance when I had nothing but my interest in stem cells and enthusiasm for research and little to no experience under my belt. I have grown a lot since then, but the current version of myself only exists because I have been given the opportunity to learn in a cutting-edge and world-class research laboratory that is the Bhatia Program.

To my committee members Dr. Anargyros Xenocostas, Dr. Andrew McArthur, and Dr. Clinton Campbell, thank you for always showing keen interest in my project and for your scientific input throughout this journey. Your participation and collaboration are what allowed me to move forward from my research questions to finally harvesting results that I hope one day would be able to help patients in a meaningful way.

To the members of the Bhatia lab, thank you for being such amazing colleagues and friends. Thank you for your constant support not only with regards to your insightful scientific input, but also for being constant rocks in my life and for reminding me that I am not alone in this journey. To my dearest mentor and friend and inspiration Allison, thank you for entertaining me in our often long and crazy discussions, scientific and personal, and for being my fellow resident MBTI-typer. To my mood charger Deanna, thank you for being such a dependable and firm person that you are, your laugh always brightens my days in the lab. To my confidante Shirley, thank you for answering all my ridiculous questions always with such patience, for being such a wonderful and kind friend that I can always rely on. To Sean and Cam, thank you for reminding me to have fun from time to time, and that a little alcohol is always good for unwinding at the end of the day. To Aaida, thank you for helping me with some of the experiments that allowed me to finish this thesis on time, and for listening to me ramble as we worked together in tissue culture.

To my best friends and soulmates Gena Markous and Meaghan Doyle, and their adorable children Bean, Aurora, and Oslo Markous, and Otis and Charlie Doyle, thank you for your constant support and unwavering love that have kept me through some of the most difficult moments in my life. I would not be where I am right now without all of you. Thank and I love you.

To my beloved friends, Yosuga, Akaza, Tomomori, Yoritomo, Nicola, Yang, Kageyuki, and Allan. All of you reminded me that there is much to look forward to in life, and that there are plenty of great days waiting for me ahead. Your words of encouragement never fail to remind me of my passion for research, and that I should never give up on my dreams. I love all of you from the bottom of my heart.

Last but not least, to my parents, cousins, uncle and aunt, thank you for your endless support and unwavering belief in me. Knowing that all of you are behind me allow me to take a step forward with pursuing a degree in science when I was still unsure about which path to take. Thank you and I love you.

Table of Contents

Descriptive Note ii
Abstract iii
Acknowledgments iv
List of Figures viii
List of Supplementary Figures viii
List of Tables ix
List of Abbreviations x
Declaration of Academic Achievement xii
1.0 Introduction 1
1.1 Normal hematopoiesis 1
1.1.1 The hematopoietic system as the quintessential stem cell model 1
1.1.2 Functional assays to assess stem and progenitor populations 2
1.2 Acute Myeloid Leukemia 3
1.2.1 Clinical diagnosis and features of Acute Myeloid Leukemia 3
1.2.2 Pathogenesis of AML 4
1.3 Challenges in AML treatment 6
1.3.1 Induction mortality in older patients 6
1.3.2 Risks associated with bone marrow transplantation 6
1.3.3 Current methods of detecting minimal residual disease 7
1.4 The bone marrow microenvironment 8
1.4.1 The role and function of the hematopoietic niche 8
1.4.2 The niche in hematopoietic malignancies 9
1.4.3 AML causes remodeling of the BM landscape 9
1.5 Mesenchymal stem cells 10
1.5.1 Definition of mesenchymal stem cells 10
1.5.2 Limitations of existing methods used to interrogate the niche and mesenchymal stem cells 10
1.5.3 Mesenchymal populations implicated in AML pathogenesis 13
1.6 BM niche targeting as a non-cell autonomous method of AML therapy 15
1.6.1 Non-cell autonomous AML treatments 15
1.6.2 BM adipocytes represent a unique subset of adipocyte population 16
1.6.3 Toxicity of PPARɤ agonists 18
1.7 Study Rationale 19

1.8 Hypothesis 20
1.9 Experimental objectives 20
2.0 Materials and Methods 21
2.1 Primary human hematopoietic samples 21
2.2 Human BM-MSC isolation and expansion 24
2.3 Human BM-MSC *in vitro* differentiation 25
2.4 Two-phase mesenchymal progenitor assay 26
2.5 Mesenchymal clone lineage tracking 27
2.6 *In vitro* Transwell co-culture assay 28
2.7 High-throughput screening of small molecules 28
2.8 Cytoplasmic and nuclear extraction from BM-MSCs 29
2.9 Western blot 30
2.10 ELISA 31
2.11 Immunophenotyping 31
2.12 Mice 32
2.13 BM tissue staining 33
2.14 Statistical analysis 33
3.0 Results 34
3.1 BM-MSCs undergo fate choice transitions and show drift towards the osteoblast lineage over passages in culture 34
3.1.1 Development of an in vitro mesenchymal CFU assay 34
3.1.2 Change in mesenchymal progenitor composition upon prolonged in vitro culturing 35
3.1.3 Construction of a mesenchymal lineage tree 37
3.1.4 Mesenchymal progenitors show varying degrees of self-renewing capacities 40
3.2 BM-MSCs from AML patients are enriched in undifferentiated progenitors, exhibit reduced self-renewing and proliferative capacity, and undergo early senescence *in vitro* 42
3.2.1 Accumulation of undifferentiated mesenchymal progenitors in AML patients 42
3.2.2 Impaired proliferative and self-renewing capacity of AML BM-MSCs 44
3.3 BM-MSCs of relapsed AML patients show heightened osteoblast activity 46
3.3.1 Increased osteoblastic potential in BM-MSCs from relapsed AML patients 46
3.4 Some factor(s) in the AML sera impairs the differentiation potential of BM-MSCs 49
3.4.1 AML sera alter fate choice of healthy mesenchymal progenitors 49
3.4.2 BM-MSCs show impaired adipogenesis capacity in the presence of AML sera 51
3.4.3 AML blasts induce an undifferentiated phenotype in mesenchymal progenitors 51

3.5 Identification of a novel adipogenesis-inducing molecule through an *in vitro* BM mesenchymal screen 53
3.5.1 Discovery of an adipogenesis-inducing compound from the Spectrum Library 53
..... 55
..... 55
3.5.2 Isoginkgetin works independently of PPARγ 56
3.6 Isoginkgetin rescues the adipogenesis potential of mesenchymal progenitors *in vitro* and promotes adipogenesis in BM of healthy mice 57
3.6.1 Isoginkgetin restores the adipogenesis capacity of mesenchymal progenitors with impaired differentiation potential 57
3.6.2 In vitro administration of Isoginkgetin corrects mesenchymal progenitor composition of relapsed AML patients to resemble those of patients in remission 60
3.6.3 Isoginkgetin increases BM adipocyte content of healthy mice 61
4.0 Discussion and Conclusion 63
5.0 Bibliography 73

List of Figures

Figure 3.1: Development of an *in vitro* mesenchymal CFU assay 35
Figure 3.2: Mesenchymal CFU assay on later passage BM-MSCs show change in progenitor composition from initial plating 37
Figure 3.3: BM mesenchymal progenitors are plastic and display a tendency to drift towards the osteoblast lineage over passages in culture 39
Figure 3.4: Undifferentiated mesenchymal progenitors exist at the bottom of the mesenchymal hierarchy and show the least proliferative capability 41
Figure 3.5: AML BM-MSCs are enriched for undifferentiated mesenchymal progenitors 43
Figure 3.6: BM-MSCs from AML patients have reduced self-renewing capacity and show early senescence *in vitro* 45
Figure 3.7: BM-MSCs from relapsed AML patients show increased osteoblast potential 48
Figure 3.8: AML sera induce a loss of differentiation capacity in mesenchymal progenitors 50
Figure 3.9: AML sera impair the adipogenesis potential of BM-MSCs 51
Figure 3.10: Introduction of leukemic blasts in culture attenuates the adipogenesis potential of BM mesenchymal cells 52
Figure 3.11: Identification a novel adipogenesis-inducing molecule through an *in vitro* BM mesenchymal screen 55
Figure 3.12: Isoginkgetin induces adipogenesis independently of PPARγ activation 57
Figure 3.13: Isoginkgetin rescues adipogenesis potential of mesenchymal progenitors *in vitro* 59
Figure 3.14: Isoginkgetin recovers the attenuated adipogenesis capacity seen upon disease regeneration 61
Figure 3.15: Isoginkgetin induces adipogenesis in BM of healthy mice 62-63

List of Supplementary Figures

Figure 3.16: Optimization of BM-MNCs seeding density for mesenchymal CFU assay 68
Figure 3.17: Optimization of basal adipocyte-osteoblast differentiation medium 69
Figure 3.18: Comparison of 7 adipogenesis outputs revealed relative activity (RA) as measured by % BODIPY+ve cells to be the best output for mining primary screen results 70
Figure 3.19: Robustness and sensitivity of adipogenesis screen on BM-MSCs 71
Figure 3.20: Isoginkgetin increases adipogenesis potential of AML and healthy BM-MSCs 72

List of Tables

Table 1: Clinical details of patient samples 21-23
Table 2: Clinical details of healthy samples 23-24
Table 3: Antibodies used for flow cytometry 31-32

List of Abbreviations

α	α-MEM	α-minimum essential medium
β	β-G2P	β-glycerol-2-phosphate
A	AA2P	Ascorbic acid-2-phosphate
	Ads	Adipocytes
	Allo-HSCT	Allogeneic hematopoietic stem cell transplantation
	AML	Acute myeloid leukemia
	APL	Acute promyelocytic leukemia
B	BAT	Brown adipose tissue
	BM	Bone marrow
	BMP	Bone morphogenic protein
	BMT	Bone marrow transplantation
	BODIPY	Boron-dipyrromethene
C	CBF	Core binding factor
	CD	Clusters of differentiation
	CEBPA	CCAAT/enhancer-binding protein alpha
	CFU	Colony forming unit
	CXCL12	C-X-C motif chemokine ligand 12
	CXCR4	C-X-C chemokine receptor type 4
D	DAPI	4’,6-diamidino-2-phenylindole
	DC	Detergent compatible
	DMEM	Dulbecco’s Modified Eagle Medium
	DMSO	Dimethyl sulfoxide
	DNMT	DNA methyltransferase
E	ELISA	Enzyme-linked immunosorbent assay
	EPO	Erythropoietin
F	FAB	French-American-British classification
	FABP4	Fatty acid-binding protein 4
	FACS	Fluorescence-activated cell sorting
	FBS	Fetal bovine serum
	FFA	Free fatty acid
	FLT-3	Fms related receptor tyrosine kinase 3
H	H&E	Hematoxylin and eosin
	H3	Histone 3
	Hif-2a	Hypoxia inducible factor 2a
	HLA	Human leukocyte antigen
	HSC	Hematopoietic stem cell
	HSCT	Hematopoietic stem cell transplantation
	HSPC	Hematopoietic stem and progenitor cell
I	IBMX	3-Isobutyl-1-methylxanthine
	ICB	Immune checkpoint blockade
	IDH	Isocitrate dehydrogenase 1
	IL-7	Interleukin-7
	iMSC3	Immortalized mesenchymal stromal cell 3
	ISCT	International Society for Cellular Therapy

	ITD	Internal tandem duplication
K	KRAS	Kirsten rat sarcoma virus
L	LAIP	Leukaemia-associated immunophenotypes
	LDA	Limiting dilution assay
	$Lepr^{+}$	Leptin receptor positive
	Lin-	Lineage-negative
M	MAT	Marrow adipose tissue
	MDS	Myelodysplastic syndrome
	MLL-AF9	Mixed-lineage leukemia-AF9
	MNC	Mononuclear cell
	MOA	Mechanism of action
	MRD	Minimal residual disease
	MSC	Mesenchymal stem/stromal cell
N	NK cells	Natural killer cells
	NOD-SCID	Non-obese diabetic-severe combined immunodeficiency
	NPM1	Nucleophosmin 1
	NR	Nuclear receptor
	NRAS	Neuroblastoma RAS viral oncogene homolog
	NSB	Non-specific binding
P	PB	Peripheral blood
	PC	Positive control
	PD-1	Programmed cell death protein 1
	PD-L1	Programmed death-ligand 1
	PFA	Paraformaldehyde
	Pln	Perilipin
	PML-RARA	Promyelocytic leukemia/retinoic acid receptor alpha
	PPARγ	Peroxisome proliferator-activated receptor gamma
R	RA	Relative activity
	RBC	Red blood cell
	RT-PCR	Real-time polymerase chain reaction
	RUNX1	Runt-related transcription factor 1
	RUNX1T1	RUNX1 partner transcriptional co-repressor 1
S	Sc-Ads	Subcutaneous adipocytes
	SCF	Stem cell factor
	scRNA-seq	Single cell RNA sequencing
	SCT	Stem cell transplantation
	SDS-PAGE	Sodium dodecyl-sulfate polyacrylamide gel electrophoresis
	STAT3	Signal transducer and activator of transcription 3
T	TET2	Tet methylcytosine dioxygenase 2
	TKD	Tyrosine kinase domain
	TP53	Tumor protein p53
	TZD	Thiazolidinedione
U	UCP1	Uncoupling protein 1
V	VE	Vascular endothelium
W	WAT	White adipose tissue
	WHO	World Health Organization

Declaration of Academic Achievement

This thesis was completed mainly by the work of Charisa Henly with the following contributions from the members of Dr. Mick Bhatia's laboratory:

- Aaida Arpa:
  - Performed mesenchymal CFU experiments on some AML samples
  - Performed western blot and ELISA from compound-treated BM-MSCs
- Dr. Allison Boyd: provided scientific input, proposed the idea for the development of the *in vitro* mesenchymal CFU assay

1.0 Introduction

1.1 Normal hematopoiesis

1.1.1 The hematopoietic system as the quintessential stem cell model

Hematopoiesis refers to the production of blood occurring postnatally in the bone marrow (BM) and is a tightly regulated process maintained by an interplay of both internal and external stimuli (Goodell, Nguyen, and Shroyer 2015; Pouzolles et al. 2016). The lifelong production of blood is heralded by hematopoietic stem cells (HSCs), a group of primitive cells sitting at the apex of the hematopoietic hierarchy, which has served as a model for stem cell biology studies for decades since their identification (Abramson, Miller, and Phillips 1977). Stereotypically, HSCs are defined by their ability to produce all lineages of blood and their ability to self-renew indefinitely, sustaining this function throughout the lifespan of an individual. HSCs maintain self-renewal and differentiation through asymmetric cell division, producing two daughter cells, one which is identical to itself and possesses the capability to form all types of hematopoietic cells, the other which is more restricted in its fate choice (Goodell, Nguyen, and Shroyer 2015; Pouzolles et al. 2016; Wognum, Eaves, and Thomas 2003). These lineage-restricted populations are hematopoietic progenitors responsible for giving rise to either mature lymphoid or myeloid cells. The lymphoid lineage produces much of the widely-known immune cells such as T-cells, B-cells, and natural killer (NK) cells, while the myeloid lineage gives rise to red blood cells (RBCs), platelets, and macrophages, among others (Goodell, Nguyen, and Shroyer 2015; Pouzolles et al. 2016).

1.1.2 Functional assays to assess stem and progenitor populations

While there have been reports of the diversity of the HSC pool, they are commonly identified by their lack of lineage-restricted markers and the presence of certain cell surface antigens (Wognum, Eaves, and Thomas 2003). $CD34^{+}CD38^{-}Lin^{-}$ and $Lin^{-}Sca\text{-}1^{+}c\text{-}kit^{+}$ are some of the markers used to define primitive hematopoietic cells in human and mice respectively, attainable either through fluorescence-activated cell sorting (FACS) or lineage depletion of BM samples (Pinho and Frenette 2019; Rundberg, Pronk, and Bryder 2015; Wognum, Eaves, and Thomas 2003). As mentioned previously, HSCs, like other multipotent stem cells, are capable of self-renewal and multilineage blood differentiation, which distinguishes them from more lineage-restricted populations. HSC capacity (self-renewal and differentiation) can be measured through *in vivo* repopulation assays i.e. serial transplantations in xenograft models, which is the "gold standard" self-renewal assay used to assess the multilineage reconstitution capacity of HSCs following stem cell transplantation (SCT) and reflect long-term HSC function (Dick et al. 1997; Rundberg, Pronk, and Bryder 2015). On the other hand, progenitor capacity can be assessed through the *in vitro* hematopoietic colony-forming unit (CFU) assay, which measures the proliferation and differentiation ability of individual cells within a hematopoietic sample (Bock 1997; Kronstein-Wiedemann and Tonn 2019). This is achievable through the quantitation of colonies (clusters of differentiated blood cells) produced by each cell with a progenitor capacity. The assay is typically ran for 14 days to allow for colonies to grow into a size that can allow for their quantitation and identification. In short, multiple, well-defined and standardized assays have been established for measuring the stem and progenitor compartments of the hematopoietic hierarchy (Bock 1997; Kronstein-Wiedemann and Tonn 2019).

1.2 Acute Myeloid Leukemia

1.2.1 Clinical diagnosis and features of Acute Myeloid Leukemia

Much of our understanding regarding stem cells comes from studies of the hematopoietic system, and correspondingly, studies of events that generate hematopoietic neoplasms such as Acute Myeloid Leukemia (AML). Similar to the hematopoietic system, AML too is organized in a hierarchical fashion. Leukemia stem cells (LSCs) sit at the top of this hierarchy and are capable of disease propagation in xenograft transplant systems (Bonnet and Dick 1997; Hope, Jin, and Dick 2004; Lapidot et al. 1994). Clinically, AML is characterized by the abnormal proliferation and differentiation of haematopoietic cells of myeloid origin. It affects predominantly individuals older than 60 years of age, and is the most common acute leukemia in adulthood, accounting for almost 80% of all cases (Kouchkovsky and Abdul-Hay 2016). The clinical manifestations of AML arise from the accumulation of immature and poorly differentiated cells, termed leukemic blasts, within the BM, peripheral blood (PB), and to a less common extent, in other organs. AML patients often present with symptoms of BM failure such as anemia, neutropenia, and thrombocytopenia, and they are also at an increased risk for infection and bleeding, which if left untreated, can usually culminate in death within months of diagnosis (Kouchkovsky and Abdul-Hay 2016). Laboratory methods used to diagnose AML typically include a complete blood count (CBC), a PB film examination, a BM aspirate, and a biopsy specimen examination, especially when the aspirate yields a dry tap. Furthermore, immunohistochemistry, flow cytometry, cytogenetics, and molecular biology analyses are likewise used to determine a diagnosis. Diagnosis for acute leukemias is generally established by the presence of 20% or more of leukemic blasts in the BM or circulating blood; however, in some cases where certain genetic abnormalities such as a t(8;21),

inv(16), or t(15;17) are observed, or in the presence of an extramedullary tissue infiltrate, a diagnosis may also be established regardless of the blast percentage (Vardiman et al. 2009).

1.2.2 Pathogenesis of AML

AML can develop in patients already diagnosed with other hematological malignancies such as myelodysplastic syndrome (MDS) and other myeloproliferative neoplasms, or manifest as a consequence of therapies that they initially receive (Arber et al. 2016; Estey 2020; Kouchkovsky and Abdul-Hay 2016). The majority of AML, however, arises as a *de novo* hematopoietic malignancy in individuals that are otherwise categorized as previously being healthy (Arber et al. 2016; Estey 2020; Kouchkovsky and Abdul-Hay 2016). For certain subtypes of AML, microscopically detectable chromosomal translocations are often implicated in the development of the disease; for example, t(8:21) in core-binding factor AML (CBF-AML) or t(15:17) in acute promyelocytic leukemia (APL), which results in the formation of chimeric proteins RUNX1-RUNX1T1 and PML-RARA respectively (Arber et al. 2016; Estey 2020; Kouchkovsky and Abdul-Hay 2016). Multiple genetic lesions without large chromosomal abnormality have also been observed and accepted to contribute to the establishment of the leukemic disease. Studies of animal models in the past few decades have led to the development of the 2-hit model for leukemogenesis and help classify the various mutations associated with the pathogenesis of AML, especially for those cases of AML with normal cytogenetics (Kouchkovsky and Abdul-Hay 2016). According to the model, leukemogenesis may occur as a result of class I mutations, which cause the activation of pro-proliferative pathways, together with class II mutations, which disrupt normal hematopoietic differentiation (Kouchkovsky and Abdul-Hay 2016). Class I mutations implicate genes such as FLT3 (mutation presented as internal tandem duplications (ITD), or in the tyrosine

kinase domain (TKD)), K/NRAS, TP53, c-kit, and STAT3 – all of which are involved in cellular proliferation and survival. Increased tyrosine phosphorylation of STAT3 or mutation in tyrosine kinase receptor e.g. FLT3-ITD are typically associated with worse prognosis for patients (Kouchkovsky and Abdul-Hay 2016). On the other hand, class II mutations such as NPM1 and CEBPA, 2 of the most common genes found to be mutated in adult AML patients and interfere with myeloid differentiation, generally confer a more favourable outcome (Kouchkovsky and Abdul-Hay 2016). Recently, a class III mutation has also been described in AML pathogenesis, which encompasses changes in the epigenetic landscape that later also affects cellular proliferation and survival. This includes mutation in DNA methylation genes such as DNMT3A, TET2, IDH-1, and IDH-2 (Kouchkovsky and Abdul-Hay 2016).

The French-American-British (FAB) classification system is the first classification system used to define the different types of AML (categorized into 8 subtypes of AML; M0 to M7), based on the morphology and cytochemistry of the leukemic cells (Kouchkovsky and Abdul-Hay 2016; Vardiman et al. 2009). Later, the World Health Organization (WHO) also introduced a new classification system for AML, which incorporates genetic information along with morphology, immunophenotype, and clinical presentation (Arber et al. 2016; Vardiman et al. 2009), resulting in 6 major subtypes of AML: 1). AML with recurrent genetic abnormalities, 2). AML with myelodysplasia-related changes, 3). Therapy-related myeloid neoplasms, 4). AML not otherwise specified, 5). Myeloid sarcoma, and lastly 6). Myeloid proliferation related to Down syndrome (Arber et al. 2016).

1.3 Challenges in AML treatment

1.3.1 Induction mortality in older patients

Following diagnosis, patients usually undergo two phases of therapy: induction chemotherapy, the goal of which is to eradicate bulk leukemic cells and for patients to achieve initial remission; and consolidation therapy, which is used to cement this state of remission. In AML, however, clinical outcome worsens with advancing age, so the management of older patients face some unique therapeutic challenges. Presently, regimens for induction chemotherapy include high doses of cytarabine- and anthracycline-based molecules. Such treatments are not well-tolerated in elderly patients, who display various comorbidities and thus show high induction mortality (Kouchkovsky and Abdul-Hay 2016). In reality, many elderly patients, who make up the majority of individuals diagnosed with AML, succumb to the disease before they can undergo bone marrow transplantation (BMT), which to this date, is the only curative method for treating AML.

1.3.2 Risks associated with bone marrow transplantation

While more chemotherapy can be given to consolidate remission in patients, bone marrow stem cell transplantation (BM-SCT), or specifically allogeneic hematopoietic stem cell transplantation (allo-HSCT), remains the only therapeutic method with the most durable effect to keep patients in remission, especially for those diagnosed with high-risk AML (Tsirigotis et al. 2016). Still, barring the success of identifying a BM donor, there are 2 significant barriers to achieving long-term survival for these patients: transplant-related mortality and its associated morbidities, as well as disease relapse. Allo-HSCT is closely associated with early and late

treatment-related mortality due to infections, toxicity, and graft-vs.-host disease, all of which remain as the main causes of death in patients (Styczyński et al. 2020).

1.3.3 Current methods of detecting minimal residual disease

Chemotherapy does not guarantee complete disease remission and in fact may provoke the emergence of leukemic clones responsible for causing relapse (Boyd et al. 2018). As much as 40% of AML patients will relapse post-SCT, and they are then faced with a dismal prognosis of a 2-year survival rate less than 20% (Bejanyan et al. 2015; Schmid et al. 2012).

Post-SCT, the objective that has become a developing niche within the treatment landscape is to perform intensive monitoring of high-risk patients. One such methodology is by evaluating the levels of minimal residual disease (MRD) in patients, which are thought to be the population of cells responsible for causing disease regeneration (Tsirigotis et al. 2016). Common MRD assays used in the clinic to identify residual leukemic cells include multi-panel flow cytometry for identification of cells carrying leukemia-associated immunophenotypes (LAIPs), RT-PCR assays for detection of fusion gene transcripts, mutated genes, overexpressed genes, and chimerism analysis, for monitoring the post-transplant engraftment of donor cells (Tsirigotis et al. 2016). To be deemed reliable, MRD assays must be highly reproducible, easily standardized across different laboratories, and show high sensitivity and specificity. The current reality is, most MRD assays used in the clinic often fall short on one of the aforementioned criteria, especially with regards to reproducibility and standardization. Due to the heterogeneous nature of AML, molecular monitoring is typically tailored to individual patients, as to avoid the risk of overlooking new leukemic clones that harbor different molecular signatures from the population first identified at

diagnosis (Tsirigotis et al. 2016). Furthermore, variations in instruments, fluorophores used, as well as an operator's gating techniques, all contribute to significant differences seen in flow cytometry results, which highlights the importance of using more than one modality in post-SCT disease surveillance (Tsirigotis et al. 2016). Together, these points summarize some of the challenges we face at present in treating AML, driving the need to identify new therapeutic and disease monitoring strategies.

1.4 The bone marrow microenvironment

1.4.1 The role and function of the hematopoietic niche

An emerging area of interest is to look at leukemia and stroma interaction in the BM. The marrow becomes the primary site of hematopoiesis postnatally and is home to HSCs responsible for lifelong production of blood (Morrison and Scadden 2014; Pinho and Frenette 2019). The stroma, also known as the niche or the marrow microenvironment, is the non-parenchymal component of the BM and is the external factor critical in regulating and maintaining the normal functioning of HSCs, including their ability to self-renew and differentiate into mature blood cells (Morrison and Scadden 2014; Pinho and Frenette 2019; Witkowski, Kousteni, and Aifantis 2019). Under homeostasis, the cellular constituents that make up the niche secrete distinct chemical signals and provide physical interactions that allow for HSC maintenance and regulation of normal blood production (Morrison and Scadden 2014; Pinho and Frenette 2019). For example, VE-cadherin^{+} vascular endothelial cells, mesenchymal stem/stromal cells (MSCs), and leptin receptor-expressing (Lepr^{+}) perivascular stromal cells secrete stem cell factor (SCF) and CXCL12, which are important factors in enforcing HSC quiescence and homing of HSCs to the marrow (Morrison and Scadden 2014; Pinho and Frenette 2019; Witkowski, Kousteni, and Aifantis 2019). Accessory

cells such as osteoblasts, specialized types of macrophages, as well as megakaryocytes have also been shown to be involved in anchoring HSCs in the marrow and maintaining their quiescence through proximal interactions. Other locally secreted factors such as interleukin 7 (IL-7) and erythropoietin (EPO) are similarly important regulators of HSC proliferation and differentiation (Morrison and Scadden 2014; Pinho and Frenette 2019; Witkowski, Kousteni, and Aifantis 2019).

1.4.2 The niche in hematopoietic malignancies

The role the niche plays in overseeing and maintaining proper hematopoiesis renders it a hotspot for many blood- and marrow-related disorders, including AML. To this day, it is still unclear whether the niche is involved in the initiation (i.e. the niche acting as a predisposition factor; gaining mutations or alterations in their function that predisposes malignancy development) or propagation of the disease (i.e. the niche acting as facilitator of malignancy; transformed hematopoietic cells alter the function of the niche, which in turn enables disease progression), and both models have been accepted as non-mutually exclusive contributors to leukemogenesis.

1.4.3 AML causes remodeling of the BM landscape

Undoubtedly, the niche undergoes some alteration – whether this is prior to disease manifestation or upon introduction of the disease – to create an environment that is conducive for malignant growth. Despite primitive subsets of AML cells and their healthy HSC counterparts sharing the same spatial localization in the niche (Boyd et al. 2014), it is apparent that disease progression extends beyond simple competition between leukemic and healthy cells, or physical crowding of the marrow. Numerous studies have shown the involvement of the niche in maintaining leukemic clones and chemotherapy resistance through the remodeling of the BM

stroma that gives rise to a unique cellular and biochemical environment specific for leukemic growth (Rashidi and Dipersio 2016; Schepers et al. 2013; Schepers, Campbell, and Passegué 2015; Witkowski, Kousteni, and Aifantis 2019).

1.5 Mesenchymal stem cells

1.5.1 Definition of mesenchymal stem cells

MSCs are integral members of the BM microenvironment, typically defined as non-haematopoietic multipotent stem cells capable of giving rise to adipocytes, osteoblasts, and chondrocytes *in vitro* (Ka et al. 2014; Morrison and Scadden 2014; Pinho and Frenette 2019; Witkowski, Kousteni, and Aifantis 2019). The existence of an entity within the BM that is distinct from HSC and capable of self-renewal and differentiation into the mesenchymal lineages was first demonstrated through the work of Friedenstein et al. (A. J. Friedenstein 1980). He and his group observed the formation of colony-forming unit fibroblasts (CFU-Fs) from BM stroma suspension (A. J. Friedenstein 1980), which are now known as MSCs. These CFU-Fs were identified based on their ability to adhere to plastic, the multipotent ability to self-renew and differentiate into the adipocyte, osteoblast, and chondrocyte lineages *in vitro,* and show hematopoietic-supporting function when re-transplanted *in vivo* (A. J. Friedenstein 1980; A. J. Friedenstein, Chailakhyan, and Gerasimov 1987; A J Friedenstein et al. 1968; A J Friedenstein, Piatetzky-Shapiro, and Petrakova 1966; Alexander J. Friedenstein et al. 1974).

1.5.2 Limitations of existing methods used to interrogate the niche and mesenchymal stem cells

Since their discovery, the CFU-F assay is a commonly used method to quantify stromal progenitors (Clarke and McCann 1989; A. J. Friedenstein, Chailakhjan, and Lalykina 1970).

Although a lot of effort has been made into looking at the stroma and MSCs since then, studies on MSCs remain very difficult to perform. This challenge is underpinned by several factors that mostly revolves around the difficulty in characterizing MSCs (Ka et al. 2014; Tikhonova et al. 2019). A gap is yet to be bridged between the hematopoietic and mesenchymal fields with regards to how their respective stem and progenitor cell populations are functionally characterized. The HSC field is equipped with multiple, well-defined assays to study the self-renewal and differentiation capacity of their primitive populations (e.g., assessment of stemness through *in vivo* repopulation and serial transplantation assays, and progenitor capacity interrogated through the hematopoietic CFU assay), whereas the MSC field is faced with the absence of such rigorous and stringent assays, especially when defining the behaviour and function of MSC at the single cell level (Bianco et al. 2013; Bianco, Robey, and Simmons 2008). Most studies in the field still rely on the derivation of a heterogeneous pool of cells – each with varying self-renewal and differentiation capacities – from high-density plated cells in culture, which does not provide an accurate depiction of MSC behaviour clonally (Bianco et al. 2013; Bianco, Robey, and Simmons 2008). Aside from that, there is no consensus to date as to which phenotypic and molecular markers should be used to define MSCs in humans, and their identification becomes reliant on their ability to adhere on plastic and proliferate *in vitro* (Dominici et al. 2006).

The International Society for Cellular Therapy (ISCT) attempted to standardize the definition of an MSC in culture by establishing a minimum set of criteria that a cell must fulfill in order to be accepted as an MSC, and these are: 1). Plastic adherence under standard tissue culture conditions, 2). The expression of CD73, CD105, and CD90, 3). Lack of expression of the surface markers CD45, CD34, CD14/CD11b, CD79/CD19 and HLA-DR, and lastly, 4). The capacity to

differentiate *in vitro* into the three mesenchymal lineages: adipocytes, osteoblasts, and chondrocytes (Dominici et al. 2006), which has been shown to differ depending on the tissue of origin (Bianco et al. 2013; Bianco, Robey, and Simmons 2008). The lack of agreement surrounding MSC phenotype also comes from the variability in cell isolation and cell culture methods that exist within the field (Leuven 2011). Source tissue, quality of plastic surface, and even miniscule differences in plating density, oxygen concentration, and media supplements all play a role in shaping the gene profile, epigenetic landscape, and behaviour of a MSC population (Leuven 2011; Sisakhtnezhad, Alimoradi, and Akrami 2017). It is also worth noting that similar to the aging phenomenon seen in cultured MSCs, BM stroma composition also changes with age *in vivo*, with BM-MSCs displaying a preference to form fat, compromising their ability to differentiate into the osteogenic lineage (Ganguly et al. 2017). In short, the age of individual from which the BM-MSCs are derived from will also contribute to the differences seen in their trilineage differentiation capacity.

Lastly, the low frequency at which MSCs exist in the marrow makes it necessary that they are expanded prior to use (Wagner et al. 2008; Whitfield et al. 2013). This is compounded by the inability of MSCs to proliferate and self-renew indefinitely *in vitro*, thereby arguably betraying their definition as a primitive population of cells. Likewise, continued serial passaging of MSCs in culture has been shown to compromise their differentiation capacity over time, which dissuades their application in regenerative medicine despite their initial premise as a promising tool for cellular therapy (Bonab et al. 2006; Wagner et al. 2008; Whitfield et al. 2013). Consistent with this finding, a comprehensive analysis of the BM stroma population in healthy mice using single-cell RNA sequencing (scRNAseq) revealed marked differences in gene expression between

cultured and freshly isolated cells (Wolock et al. 2019). Cultured cells showed expression profiles resembling that of osteoprogenitors, while only a subset of the cultured population retained recognizable MSC expression (Wolock et al. 2019). This illustrates the disparity in both morphology and differentiation capacity that are commonly observed in culture-expanded MSCs, although the source and consequence of such heterogeneity are still not much understood (Whitfield et al. 2013). Transcriptional trajectories of MSC differentiation from this study also pointed to the existence of a subset of stromal populations that are more-lineage restricted, some with bipotential capacity, which are reminiscent of progenitors that exist within hematopoietic hierarchies (Wolock et al. 2019). This finding suggests that the onset of MSC heterogeneity may exist early on and perhaps is not a simple consequence of prolonged culture.

1.5.3 Mesenchymal populations implicated in AML pathogenesis

Further complicating the matter, while it is clear AML dramatically perturbs the architecture and function of MSCs, the disturbance imposed on specific mesenchymal lineages are inconsistent across different studies. An interrogation of stromal population in BM of mice during homeostasis and leukemia (AML originating from MLL-AF9 translocation) using scRNAseq showed the decreased propensity of MSCs towards the adipogenic and osteogenic lineages (Baryawno et al. 2019). The cell profiles of these MSCs suggest an undifferentiated state stemming from the activation of hypoxia pathway genes (Rauner et al. 2016). Other studies have shown similar findings of impairment of osteogenesis and decreased osteoblast activity in AML, which in turn accelerates leukemic progression (Frisch et al. 2012; Hanoun et al. 2014; Krevvata et al. 2014; B Kumar et al. 2018), while some reported the opposite observation, demonstrating

instead the increased osteogenic potential of BM-MSCs via BMP-mediated signaling, leading to enhanced leukemic engraftment in mice (Battula et al. 2017; Schepers et al. 2013).

Adipocytes have always been deemed as a negative regulator of hematopoiesis and HSCs (Naveiras et al. 2009); their accumulation in the BM in aging and obese individuals thought to impair regeneration of both hematopoietic cells and bone (Ambrosi et al. 2017). Various studies have shown the enhanced propensity of BM-MSCs derived from AML patients to differentiate towards the adipogenic lineage (Azadniv et al. 2019a). Many argue that adipocytes promote AML blasts survival through the production of free fatty acids (FFA), thus contributing to propagation of the disease (Azadniv et al. 2019a; Bijender Kumar et al. 2018; Shafat et al. 2017). However, impairment of BM adipogenesis has been described in many leukemias including AML, and restoration of the adipocyte landscape within the marrow of AML-engrafted mice has in fact been shown to rescue healthy myelo-erythropoiesis while limiting leukemic progression (Boyd et al. 2017). A different study has also demonstrated the importance of BM adipocytes in maintaining HSC and hematopoiesis regeneration through the secretion of SCF following injury such as myeloablation (Zhou et al. 2017), further adding to the discrepancy seen with regards to the role BM adipocytes play.

Notably, most of the aforementioned studies observed changes on MSC function under the umbrella of AML; however, depending on the genetics and phenotype of the leukemia model used in the study, it can be gleaned that their perturbance on the hematopoietic niche will differ. Considering the heterogeneous nature of AML itself, this would add to the adversity when studying and targeting leukemic-stroma interaction, as different mechanisms might be in play. To

this date, the dynamics of how the niche, AML cells, and other healthy cells residing in the BM interact and impact healthy hematopoiesis remain poorly understood.

1.6 BM niche targeting as a non-cell autonomous method of AML therapy

1.6.1 Non-cell autonomous AML treatments

Much of the non-cell autonomous therapies currently used in the field target the leukemic microenvironment with the goal of eventually eradicating the disease. For example, the CXCR4/CXCL12 axis, which is a highly known pathway regulating HSC homing, has been shown previously to play an important role in the survival of leukemic blasts (Passaro et al. 2015; Pitt et al. 2015; Sison and Brown 2011). Plerixafor, an inhibitor of CXCR4, was shown to successfully mobilize leukemic blasts out of their niche, which increases their sensitivity to cytotoxic chemotherapies (Witkowski, Kousteni, and Aifantis 2019). Therapies targeting adipocytes through inhibition of FABP4, a carrier protein that facilitates FFA transfer from adipocytes to leukemic blasts and thought to contribute to enhancing disease progression in AML, have also been developed in recent years (Azadniv et al. 2019b, 2019a; Shafat et al. 2017; Tabe, Konopleva, and Andreeff 2020; Witkowski, Kousteni, and Aifantis 2019; Zinngrebe, Debatin, and Fischer-Posovszky 2020). Some methods seek to target the immunosuppressive microenvironment of AML instead. The use of hypomethylating agents such as azacytidine has been shown to previously upregulate the expression of immune checkpoints such as PD-1 and PD-L1 in AML. Suppressing these pathways through immune checkpoint blockade (ICB) therapies, in conjunction with azacytidine, has resulted in enhanced anti-leukemic responses (Daver et al. 2019). Immune evasion also poses a challenging hurdle to overcome in AML. For example, some AML-initiating cells express CD47 on their surface which allows them to escape phagocytosis by innate immune

cells and is a marker of poor prognosis in AML patients (Jaiswal et al. 2009; Majeti et al. 2009). Monoclonal antibodies against CD47 have been developed (Majeti et al. 2009) to reverse this evasion and shown to help promote phagocytosis of these leukemia-initiating cells, exhibiting promising anti-tumour results in early human AML clinical trials (Witkowski, Kousteni, and Aifantis 2019).

The interaction between host and tumour cells is undoubtedly critical in the survival and proliferation of the disease; thus, targeting this interaction becomes a logical next step. However, what these treatments fail to address is the issue of the remodeling of the host landscape, which in the case of AML, has not only created a hostile environment that is conducive for leukemia growth, but also one that does not support normal hematopoietic functions. Patients often suffer adverse symptoms of bone marrow failure which makes them unable to tolerate intensive chemotherapies for a long period of time, leading to their succumbing to the illness before complete eradication of the disease or receiving bone marrow transplant. The damage borne by the niche due to the disease – and to some extent, from cytotoxic chemotherapies as well – remains unaddressed.

1.6.2 BM adipocytes represent a unique subset of adipocyte population

Despite their controversial role, emerging studies have shown that adipocytes are not mere decorations posing as empty spaces within the marrow, and in fact bears a more pleiotropic role as a constituent of the hematopoietic niche. Most of the adipocyte population that resides within the BM, referred to as marrow adipose tissue (MAT), is thought to transition between white adipose tissue (WAT) and brown adipose tissue (BAT) phenotypes, which are the 2 major adipocyte cell populations found outside of the BM (Hardouin, Rharass, and Lucas 2016;

Horowitz et al. 2017; Nakagami 2013; Trayhurn and Beattie 2001). WAT is dispersed throughout the body in subcutaneous and visceral regions, with its role primarily being energy storage and as an endocrine as well as a secretory organ (Horowitz et al. 2017). Brown adipocytes on the other hand are much less abundant compared to WAT. They express uncoupling-protein 1 (UCP1) and are typically high in mitochondria, which allows them to metabolize fatty acids and generate heat upon exposure to cold (Horowitz et al. 2017; Moisan et al. 2015; Nakagami 2013).

Unlike these 2 major adipose deposits, MAT has a distinct genetic and metabolic profile from both WAT and BAT (having originated from BM-MSCs) (Attané et al. 2020), and is more closely related to osteoblasts (Horowitz et al. 2017). Its characteristics might resemble that more of beige adipocytes, as it still functions as a fatty acid regulator which is typical of WAT (José Albuquerque de Paula and J. Rosen 2018), but its putative role in iron trafficking suggests that it might also adopt similar characteristics to BAT (Boyd et al. 2017). While MAT, or BM adipocytes, share morphological features with WAT, they are geared towards a cholesterol-oriented metabolism and are devoid of lipolytic activity that are commonly seen in WAT of subcutaneous or visceral origins (Attané et al. 2020). Unlike MAT, WAT works through a glucose and fatty acid metabolism with a primary role of breaking down triglycerides and releasing FFAs (lipolysis). Interestingly, primary BM-MSCs differentiated *in vitro* to adipocytes fail to recapitulate the unique *in vivo* characteristic of MAT and are in fact more similar to the canonical WAT seen in other parts of the body (Attané et al. 2020), which renders current *in vitro* adipocyte differentiation assays unsuitable models for studying BM adipocytes.

1.6.3 Toxicity of PPARɤ agonists

GW1929, a pro-adipogenic agent that belongs to a class of thiazolidinediones (TZDs), has been found to effectively induce adipogenic differentiation of MSCs and suppressing leukemic growth, albeit minimally (Boyd et al. 2017). GW1929 induces adipogenesis by acting as a potent agonist of Peroxisome proliferator-activated receptor γ (PPARγ), a transcription factor belonging to the nuclear receptor (NR) superfamily and a master regulator of adipogenesis (Farmer 2006; Lefterova et al. 2014; Lehrke and Lazar 2005; Lowell 1999). However, most PPARγ agonists have been shown to exert toxic side effects when administered at high doses in animals (Home 2011). For example, Rezulin (i.e. Troglitazone), another drug which acts as a PPARγ agonist and was initially approved for the treatment of type II diabetes, has been withdrawn from the market due to hepatotoxicity issues (Smith 2003). The effort to find novel compounds that can induce adipogenesis in the marrow, independently of PPARγ, proves to be a difficult task to perform as PPARγ has been proven by numerous studies to be necessary in adipose tissue differentiation, both *in vivo* and *in vitro* (Rosen et al. 1999). Despite being functionally and metabolically distinct from other adipose tissues in the body, the biomolecular mechanisms regulating MAT differentiation might not be different from normal white and brown adipocytes differentiation; for example, the dependence on PPARγ (Imai et al. 2004). However, as MAT resides within the BM, its interaction with HSCs and other niche cells makes it a unique subset of adipose depot that may allow us to preferentially target the BM adipocyte niche with minimum side effects on haematopoietic cells, non-adipocytic BM niche cells, or other adipose deposits located outside of the BM.

1.7 Study Rationale

AML is a disease of primarily the elderly who are unable to tolerate intensive chemotherapy and often show early induction mortality. BMT, which is used to consolidate remission following induction therapy, comes with significant morbidity and transplant-related mortality, as well as the risk of the disease returning following transplantation. Currently, the clinics have shifted strategies towards performing intensive monitoring of high-risk patients, specifically by evaluating the levels of MRD, which are thought to be the population of cells responsible for causing relapse in patients. However, MRD assays used in the clinic to this date remain insufficient in capturing the onset of disease regeneration and they are not easily standardized across different laboratories, especially when used to measure a heterogeneous disease such as AML. Together, these points present some of the biggest challenges currently faced in the treatment of AML, driving the need to identify new therapeutic and disease monitoring strategies.

In recent years, many have turned to looking at leukemia-stroma interactions in the BM in their effort to develop non-cell autonomous AML therapeutic strategies. The stroma, or the BM niche, is a specialized microenvironment critical in maintaining and regulating normal hematopoiesis, which undergoes remodeling during malignant states such as AML. This damage is further exacerbated by the numerous rounds of myeloablative regimens received by patients that are initially intended to target diseased cells. The damage incurred by the niche becomes an issue that must be delineated and addressed in the current therapeutic landscape, as most niche-based interventions focus solely on eliminating the disease. Furthermore, study on niche populations such as mesenchymal cells is challenging and often limited to *in vitro* expansion of colony

outgrowths and differentiation assays, which fail to demonstrate their complexity and their contribution to disease pathology. As of this moment, our understanding of how mesenchymal cells and their progenies are implicated in AML remain largely incomplete.

1.8 Hypothesis

It is hypothesized that the AML BM niche (specifically mesenchymal cells and their progenies) is perturbed upon introduction of the leukemic disease and that repair of the niche would support the patient's *de novo* hematopoiesis, which in turn would increase their survival and the success of BM-SCT; 2). There exists a unique pattern in the AML mesenchymal niche associated with remission versus relapse outcomes that can be utilized to improve current methods of detecting MRD and as an early intervention of disease regeneration.

1.9 Experimental objectives

This thesis aims to:

1. Characterize the functional impairment of AML BM-MSCs *in vitro* using a novel mesenchymal CFU assay.
2. Determine whether BM-MSC of patients who successfully achieved remission are functionally different from those who relapsed.
3. Determine whether pharmacological modulation would be able to reverse or repair the aberrations observed in the leukemic niche.

2.0 Materials and Methods

2.1 Primary human hematopoietic samples

Human haematopoietic cells were obtained from BM aspirates of adult donors or AML patients. All AML haematopoietic cells were provided by Juravinski Hospital and Cancer Centre and London Health Sciences Centre (University of Western Ontario) from informed consenting patients in accordance with approved protocols by the Research Ethics Board at McMaster University and the London Health Sciences Centre, University of Western Ontario. Healthy hematopoietic cells were either purchased from Discovery Life Sciences or acquired from London Health Sciences Centre with same approved protocols as mentioned above. Details of AML patient and healthy donor samples were outlined in Table 1 and 2 respectively. Using a previously established protocol, mononuclear cells (MNCs) were isolated using density gradient separation (Ficoll-Paque Premium, GE Healthcare) followed by red blood cell lysis using ammonium chloride solution (Stemcell Technologies). Cells were cryopreserved in 90% FBS with 10% DMSO for long-term storage in liquid nitrogen.

Table 1. Clinical details of patient samples

Patient ID	Disease stage	Sample	Age	Sex	Cytogenetics/Molecular
AML 1	Diagnosis	BM-MNCs	74	Male	46,XY [13], FLT3-ITD
AML 2	Diagnosis	BM-MNCs	73	Female	Inconclusive/not tested
AML 3	Diagnosis	BM-MNCs	68	Female	Inconclusive/not tested
AML 4	Diagnosis	BM-MNCs	66	Male	45,X,-Y,t(9;11)(p22;q23)[23]/46,XY[2]
AML 4.1	Remission	BM-MNCs	66	Male	45,X,-Y,t(9;11)(p22;q23)[23]/46,XY[2]

AML 4.2	Relapse	BM-MNCs	66	Male	45,X,-Y,t(9;11)(p22;q23)[23]/46,XY[2]
AML 5	Diagnosis	BM-MNCs	61	Female	46,XX[14]
AML 5.1	Remission	BM-MNCs	61	Female	46,XX[14]
AML 5.2	Remission	BM-MNCs	61	Female	46,XX[14]
AML 6	Diagnosis	BM-MNCs	48	Female	46,XX[25], NPM1, FLT3 D835
AML 7	Diagnosis	BM-MNCs	41	Male	Cytogenetics N/A, CBFß/MYH11, CKIT
AML 8	Diagnosis	BM-MNCs	34	Female	45~46,XX,der(X)?t(X;11)(q28;q12)[2],-2[3],del(3)(q11.2)[3],-5[2],add(7)(p11.2)[3],-17[3],+3~5mar[3][cp3]
AML 9	Diagnosis	BM-MNCs	28	Male	46,XY[20] , NPM1
AML 10	Diagnosis	BM-MNCs	28	Female	N/A
AML 10.1	Follow-up	BM-MNCs	28	Female	N/A
AML 10.2	Remission	BM-MNCs	28	Female	N/A
AML 11	Diagnosis	BM-MNCs	23	Male	N/A
AML 12	Diagnosis	BM-MNCs	29	Female	N/A
AML 13	Diagnosis	BM-MNCs	29	Female	N/A
AML 14	Relapse	BM-MNCs	73	Male	46,XY[20]
AML 15	Pre-induction (treatment with HU)	BM-MNCs	58	Male	Normal karyotype
AML 16	Pre-induction	PB serum	68	N/A	N/A
AML 17	Pre-treatment	PB serum	76	Female	N/A
AML 18	Pre-treatment	PB serum	34	Female	N/A
AML 19	Pre-treatment	PB serum	24	Female	N/A

AML 20	Pre-treatment	PB serum	72	Female	N/A
AML 21	Post-diagnostic	Leukapheresis	78	Female	N/A
AML 22.2	Remission	BM-MNCs	62	Male	N/A
AML 22.3	Follow-up Remission	BM-MNCs	62	Male	N/A
AML 23	Remission	BM-MNCs	55	Female	N/A
AML 23.1	Remission	BM-MNCs	55	Female	N/A
AML 24.1	Partial remission	BM-MNCs	69	Male	N/A
AML 24.2	Remission	BM-MNCs	69	Male	N/A
AML 24.3	Relapse	BM-MNCs	69	Male	N/A
AML 25.1	Remission	BM-MNCs	63	Female	N/A
AML 25.2	Relapse	BM-MNCs	63	Female	N/A
AML 26.1	Diagnosis	BM-MNCs	63	Female	46,XX,del(16)(q13q23)[5]/45, XX[19]
AML 26.4	Relapse	BM-MNCs	63	Female	46,XX,del(16)(q13q23)[5]/45, XX[19]
AML 26.5	Relapse	BM-MNCs	63	Female	46,XX,del(16)(q13q23)[5]/45, XX[19]

Table S2. Clinical details of healthy samples

Donor ID	Disease stage	Sample	Age	Sex	Cytogenetics/Molecular
Healthy 1	Normal	BM-MNCs	32	Male	N/A
Healthy 2	Normal	BM-MNCs	73	Female	N/A
Healthy 3	Normal	BM-MNCs	71	Female	N/A
Healthy 4	Normal	BM-MNCs	66	Male	N/A
Healthy 5	Normal	BM-MNCs	61	Male	N/A

Healthy 6	Normal	BM-MNCs	60	Female	N/A
Healthy 7	Normal	BM-MNCs	55	Male	N/A
Healthy 8	Normal	BM-MNCs	30	Male	N/A
Healthy 9	Normal	BM-MNCs	N/A	N/A	N/A
Healthy 10	Normal	BM-MNCs	N/A	N/A	N/A
Healthy 11	Normal	PB serum	N/A	N/A	N/A
Healthy 12	Normal	PB serum	N/A	N/A	N/A
Healthy 13	Normal	BM-MNCs	N/A	N/A	N/A
Healthy 14	Normal	BM-MSCs	N/A	N/A	N/A

2.2 Human BM-MSC isolation and expansion

BM mononuclear cells (BM-MNCs) were plated into a T150 flask (Corning, TC-treated) at a density of 200,000 cells/cm^2. Cells were suspended in non-haematopoietic media consisting of α-MEM (Gibco) supplemented with 10% Fetal Bovine Serum (FBS, Wisent Inc.) and 1X L-glutamine (Life Technologies). The culture was left undisturbed for a few days to allow for attachment of MSCs, and after 5 days, an equal volume of fresh media was added. The cells were continued to be grown in culture until they reach approximately 80% confluency, with a complete media change performed every 2-3 days. Afterwards, adherent cells were dissociated using TrypLE, and the cells were deprived of CD45$^+$ haematopoietic cells using EasySepTM Human CD45 Depletion Kit II (Stemcell Technologies), before re-plated into a new flask at a density of 10,000/cm^2. As proposed by the International Society for Cellular Therapy, ≥95% of the isolated cells were confirmed using flow cytometry to express the common MSC markers CD105, CD73, and CD90, and lack the expression of CD45, CD34, and CD14.

2.3 Human BM-MSC *in vitro* differentiation

BM-MSCs were induced towards the adipogenic and osteogenic lineages after the culture reached 70-80% confluency. For adipocyte differentiation, the cells were cultured in basal adipogenesis induction medium consisting of DMEM (Gibco) supplemented with 2% FBS, 500 µM 3-Isobutyl-1-methylxanthine (IBMX, Sigma-Aldrich), 1 µM dexamethasone, and 5 µg/mL insulin (BioLegend). Titration of reagents allowing minimum level of adipogenesis has been previously determined (Supplementary Fig. 3.17a), and the composition was chosen on the basis of assay sensitivity as measured by Z' score (Supplementary Fig. 3.17b). Differentiation media was replaced every 2-3 days for 9 days. At day 9, the cells were fixed with 2% paraformaldehyde (PFA) and stained with 20 µM boron-dipyrromethene (BODIPY, ThermoFisher Scientific) as well as 1:1000 Hoechst (Life Technologies) at room temperature for 45 minutes. Cells were imaged at 10x magnification using Operetta high-content imaging system (Perkin Elmer). Whole well images of the culture were stitched and stored online using Columbus image data storage and analysis system (Perkin Elmer). Media cocktail for osteoblastogenesis follows protocol from Millipore Sigma (Supplementary Fig. 3.17c) and contains 10% FBS, 1 µM dexamethasone, 0.2 mM ascorbic acid 2-phosphate (Sigma-Aldrich), 10 mM β-glycerol-2-phosphate (Sigma-Aldrich), and 1X L-glutamine in DMEM (Gibco). Culture was induced for osteoblast differentiation for a total of 18 days, with media change performed every 2-3 days. After 18 days of osteogenic induction, cells were fixed with 2% PFA and stained with Alizarin red S solution (Millipore Sigma) for 25 minutes at room temperature in the dark. Following staining, cells were washed 2-3 times with 1X PBS to remove any excess dye. Representative colour brightfield images were taken at 4X using standard filter sets on ToupView imaging software.

2.4 Two-phase mesenchymal progenitor assay

The mesenchymal progenitor capacity of each BM sample was evaluated using a mesenchymal colony-forming unit (CFU) assay. At the start of the expansion phase, BM-MNCs were plated onto a 6-well plate at a density between 0.05 - 0.1 x 10^6 cells/well or approximately 5,000-10,000 cells/cm^2 for samples from healthy donors, and 0.5 - 1.0 x 10^6 cells/well or 50,000 - 100,000 cells/cm^2 for samples derived from AML patients. Limiting dilution assays were usually performed for new samples tested, however the aforementioned range of cell seeding densities were found to give rise to colonies with optimum number for counting and typing healthy and AML BM mesenchymal samples respectively (Supplementary Fig. 3.16). The cells were suspended in non-haematopoietic media (α-MEM + 10% FBS), and were left undisturbed for 5 days to allow for attachment. At day 5, an equal volume of media was added to the culture, before they were expanded for an additional week. During this expansion period, full media changes were performed every 2-3 days. In the differentiation phase at day 12, the cells were introduced to a basal medium that is permissive for both adipocyte and osteoblast differentiation. The adipo-osteo basal induction medium consists of reagents required for both mesenchymal differentiation processes and contains 10% FBS, 500 µM IBMX, 5 µg/mL insulin, 1 µM dexamethasone, 0.2 mM ascorbic acid 2-phosphate, 10 mM β-glycerol 2-phosphate, and 1X L-glutamine in DMEM. Osteoblastogenesis generally takes longer time to occur than adipogenesis, therefore to compensate for the shorter differentiation period, the reagents for osteoblast differentiation are set at the typical concentration used for full osteoblast differentiation, and this particular cocktail of medium has been confirmed to allow for osteoblast differentiation without severely compromising the adipogenesis capacity of BM-MSCs (Supplementary Fig. 3.17c). Differentiation was initiated

for a total of 9 days, and medium was replenished every 2-3 days. Cells were fixed with 2% PFA and subsequently stained with 20 μM BODIPY and 1:1000 Hoechst in DMEM. Fluorescent CFU images of live progenitors were acquired at 2x using the Operetta high-content imaging system (Perkin Elmer), and whole well images were stitched using Columbus image data storage and analysis software (Perkin Elmer). CFU images were also acquired using ChemiDoc imaging system (BioRad), using protocols previously optimized for Coomassie Blue staining (for image capture of all live colonies).

2.5 Mesenchymal clone lineage tracking

Mesenchymal clones were subjected to differentiation at multiple passages to note for the fidelity of their fate choice over time in culture. Bulk BM-MNCs were plated onto a 6-well plate and left undisturbed for 5 days before an equal amount of culture medium was added (density of cell plating and media composition were listed previously under *Methods: two-phase human mesenchymal progenitor assay*). The cells were cultured for another week, with full media changes performed every 2-3 days. Once the colonies have grown into a considerable size, they were plucked and transferred into a 96-well plate, each well containing a single colony. These cells were marked as passage 1 cells, and grown until they reach 70-80% confluency, before they were split into two identical wells marked as passage 2. One well was designated for further expansion, while the other was subjected to differentiation in a basal adipocyte-osteoblast differentiation medium (detailed medium composition listed under *Methods: two-phase human mesenchymal progenitor assay*), which allowed for tracking of the clones' fate choice at each passage number and their continued expansion in culture. The process was repeated over multiple passages, until the last mesenchymal clone ceased to proliferate.

2.6 *In vitro* Transwell co-culture assay

The adipogenesis and osteoblastogenesis potential of healthy mesenchymal cells were assessed in the presence of leukemic blasts, using Transwell inserts with 0.4 μm pores (Corning). Bulk BM-MNCs from a healthy donor were seeded into a 6-well plate, and upon formation of colony outgrowths, basal differentiation cocktail (as described previously in *Method: two-phase mesenchymal progenitor assay*) was added to the lower chamber, while leukemic cells were added to the upper Transwell chamber. A total of 2.5×10^6 viable AML blasts were added to the upper chamber of the co-culture system, and the cells were replenished every two to three days when medium change takes place. Following 9 days of differentiation and co-culture, mesenchymal progenitors were stained with Alizarin red and colony output as well as type were noted and tabulated by eyes.

2.7 High-throughput screening of small molecules

High-throughput chemical screening of 2560 molecules from the Spectrum Collection, consisting of various bioactive compounds and natural products, was performed on immortalized human bone marrow mesenchymal stromal cells – hTERT iMSC3 (abm, Cat#T0529) for their ability to induce differentiation of iMSC3s into adipocytes. The library was purchased from MicroSource as 10 mM DMSO solution in 96-well microplates at 125 μL. iMSC3s were seeded into a 96-well plate, expanded for 2 days to reach approximately 70% confluency, before they were treated 4 times with compounds from the screening library diluted 1:1000 at a final concentration of 10 μM in the adipo-osteo basal differentiation media over a period of 10 days. At day 10, the cells were fixed with 2% PFA at room temperature for 15 minutes, and then stained

with 1:1000 Hoechst and 20 μM BODIPY for 45 minutes at room temperature. Following previously established protocol, the cells were imaged using Operetta high-content imaging system at 10x magnification and analyzed on Columbus using a custom script. Adipogenesis-promoting capacity was represented as relative activity (RA), measured in terms of BODIPY+ve cells out of total live cells, as analyses of all adipogenesis outputs from 5 representative plates revealed relative activity (of %BODIPY+ve cells) to be the output that encompassed most of our criteria (Supplementary Fig. 3.18). The standard for a hit was determined previously to be three times standard deviation above the RA mean of our empty DMSO control, calculated manually for each plate. The set of hits obtained from this primary screen were further assessed for their effects on cell viability and ability to induce adipogenesis on primary human BM-MSCs derived from a healthy donor and AML patient in a dose response format.

2.8 Cytoplasmic and nuclear extraction from BM-MSCs

Healthy and AML BM-MSCs were cultured in MSC media (α-MEM supplemented with 10% FBS) up to passage 8, before they were seeded into 6 well plates, 3 plates each for every treatment condition, giving rise to approximately 30 x 10^6 viable cells during time of harvest. Undifferentiated condition refers to BM-MSCs grown in regular MSC expansion media. Basal adipogenesis differentiation cocktail has been previously determined (Supplementary Fig. 3.17a, b) and contained 0.1% DMSO which denotes empty vehicle control. GW1929 and Troglitazone were used as positive controls for adipogenesis induction. All molecules were administered at 0.08 μM, which was the EC_{50} value for Isoginkgetin. The cells were allowed to differentiate for 9 days and then scraped using cell scrapers. Nuclear and cytoplasmic protein was extracted using Cayman's Nuclear Extraction Kit (10009277) as per manufacturer's instructions except for the

following changes: following addition of the hypotonic buffer to the cell pellet, the cells were incubated for 10 minutes, resuspended by pipetting, and incubated for another 10 minutes. The manufacturer's protocol was then resumed and the cytoplasmic supernatant was extracted after incubation with the hypotonic buffer, addition of NP-40 Assay Reagent and subsequent centrifugation. The remaining pellet was processed further to obtain the nuclear extract. The cytoplasmic and nuclear extracts were flash frozen and stored in -80 °C before use.

2.9 Western blot

The protein concentrations in both the nuclear and cytoplasmic extracts were quantified using a DC assay using the DC Protein Assay (BIORAD 5000111). A total of 30 µg of protein was used for each sample to run a Western blot. The cytoplasmic and nuclear extracts were treated with Laemmli with 2-mercaptoethanol, boiled at 95 °C for 10 minutes, separated by SDS–PAGE (12.5% polyacrylamide) and transferred onto nitrocellulose membranes. The membranes were blocked in PBS containing 5% skimmed milk and 0.1% TWEEN-20 overnight, and incubated with rabbit polyclonal anti-PPARγ (Abcam, ab45036, 1:1000), mouse monoclonal anti-Actin (Millipore, no. MAB1501, 1:80,000) and rabbit polyclonal anti-H3 (Abcam, ab1791, 1:1000) primary antibodies at 4 °C for 1 hour. HRP-conjugated secondary antibodies were used at 1:50,000 (anti-rabbit: no. 1706515, anti-mouse: no. 1721011; Bio-Rad). Protein signal was developed using Immobilon ECL detection kit (Millipore). Images were acquired using a ChemiDoc XRS + System with Image Lab Software (Bio-Rad) and analyzed using Biorad Image Lab Analysis Software. The relative band intensity was observed as a ratio of the PPARγ band intensity to the H3 band intensity.

2.10 ELISA

The activity of PPARɣ in each treatment was determined by conducting an ELISA. The Cayman's PPARɣ transcription factor assay kit was used as per manufacturer's instructions except for the following changes. The recommended volume of nuclear extracts was 10 µL, however, to ensure that 30 µg was used for the assay for each sample, this volume was increased to 30 µL. To account for the higher volume of sample added, the Complete Transcription Factor Binding Assay Buffer was concentrated and 70 µL was added to the assay (total volume still remains 100 µL for every sample). The absorbance of each sample was read at 450 nm and obtained using the Floustar Omega plate reader (BMG Labtech) and Omega Analysis Software (version: 5.11). Quantitative analysis of the absorbance values were conducted using the positive control (PC) and the non specific binding control (NSB) which were both provided in the kit. Each reading was blank corrected, and then divided by the NSB for fold-change analysis with the basal medium control.

2.11 Immunophenotyping

Human BM-MSCs were identified using monoclonal antibodies against CD73, CD90, and CD105. Human hematopoietic cells (MNCs) isolated from BM aspirates were phenotyped using human-specific antibodies to detect CD45, HLA-A2, CD33, CD19, CD15, CD34, CD71 and CD16. Table 2 provides details on antibody clones, suppliers and dilutions. 7AAD was used to separate viable from non-viable cells. FACS data were acquired on CytoFLEX Flow Cytometer (Beckman Coulter) and analysed with FlowJo Software (version 9.3.2, Tree Star).

Table 2: Antibodies used for extracellular flow cytometry

Antigen specificity	Clone	Conjugation	Dilution	Catalog #	Supplier
Human CD45		APC	1:100	340943	BD Biosciences

	v450	1:100	560367	BD Biosciences
Human CD34	FITC	1:100	555821	BD Biosciences
	PE	1:200	550761	BD Biosciences
Human CD14	PE	1:100	IM0650U	Beckman Coulter
Human CD33	APC	1:300	551378	BD Biosciences
Human CD19	FITC	1:100	555412	BD Biosciences
Human CD105	PE	1:3000	560839	BD Biosciences
Human CD90	PE-Cy-7	1:3000	561558	BD Biosciences
Human CD73	Bright violet	1:500	562430	BD Biosciences
7AAD		1:50	A07704	Beckman Coulter

2.12 Mice

NOD-SCID (NOD.CB17-*Prkdc*^{scid}/J) mice were brought in from The Jackson Laboratory and were maintained in the Stem Cell and Cancer Research Institute (SCC-RI) animal barrier facility at McMaster University. All experiments were approved by the Animal Care Council of McMaster University and were in accordance with relevant ethical regulations concerning animal research. As the experiment sought to investigate BM adipocyte content upon pharmacological modulation, we have confirmed that the strain does not develop diabetes and has normal glucose homeostasis. Mice aged 16 weeks old were treated daily through oral gavage with 10% DMSO in corn oil (vehicle group), 5 mg kg^{-1} GW1929 (Cayman Chemical, cat#13689), or 20mg kg-1 Isoginkgetin (Tocris, cat#6483) for a period of 4 weeks. Whole femurs were collected and stored in 4% paraformaldehyde at room temperature overnight, for histology and immunostaining.

2.13 BM tissue staining

Femurs from NOD/SCID mice were fixed with PFA and stored in formic-acid containing Immunocal solution (Immunotec) overnight for decalcification. The decalcified mouse femurs were then paraffin-embedded and sectioned at 5 μm. Hematoxylin and eosin staining (H&E) was performed to look at the bone marrow landscape of the tissue sections. Immunofluorescence staining using Perilipin was performed to visualize adipocytes. Prior to performing antigen-retrieval, tissue sections were deparaffinized and rehydrated. Antigen-retrieval was performed by submerging the tissue sections in antigen-retrieval buffer, diluted 1:100, at 60^{o}C overnight. The following day, tissue sections were blocked using 20% donkey serum, for 1 hour at room temperature, before incubated overnight at 4^{o}C with a primary rabbit anti-mouse for detection of perilipin (1:100, Cell Signalling). The tissue sections were then stained with donkey secondary antibodies conjugated to Alexa-568 or Alexa-647 for 30 min-1 hour in the dark, before they were stained with DAPI (Invitrogen) for detection of live nuclei.

2.14 Statistical analysis

All results are represented as means ± SEM, unless stated otherwise. Prism 8 (GraphPad Software, Inc.) was used to create graphs and perform most statistical analyses. Most column and grouped analyses are assessed by unpaired Student's *t*-test, Welch's *t*-test, Mann-Whitney test, or one-way ANOVA with Tukey's multiple comparisons test when the assumptions are met. Other comparisons involved paired Student's *t*-test when comparing the effects of AML sera on the differentiation capacity of paired mesenchymal clones, and categorical analysis on mesenchymal progenitor type was done using a chi-square test calculator

(https://www.socscistatistics.com/tests/chisquare2/default2.aspx). The criterion for significance was $P<0.05$, and all *t*-tests were two-tailed unless otherwise indicated.

3.0 Results

3.1 BM-MSCs undergo fate choice transitions and show drift towards the osteoblast lineage over passages in culture

3.1.1 Development of an in vitro *mesenchymal CFU assay*

To better examine the differentiation capacity of BM mesenchymal populations from AML patients and assess how they differ from healthy individuals, we devised a novel mesenchymal CFU assay that will allow us to interrogate the differentiation capacity of each sample at the progenitor level. Following plating of BM mononuclear cells (BM-MNCs) onto plastic surface, we observed for adherence of fibroblastic populations. These fibroblastic attachments were expanded over a period of 12 days to allow for formation of colony outgrowths, before they were exposed to a basal differentiation cocktail that is permissive of differentiation into adipocytes and osteoblasts (Fig. 3.1a), making our assay the first in the field to assess both mesenchymal lineages simultaneously. At the end of the assay, colonies that still displayed fibroblastic phenotype and showed no calcium mineralization nor lipid droplets formation were noted as undifferentiated progenitors (CFU-Us) (Fig. 3.1b). Osteoblast colonies (CFU-Os) displayed mineralization that is typical of osteoblast differentiation and showed Alizarin red S staining (Fig. 3.1b). Both CFU-U and CFU-O were marked as $Hoechst^{+}BODIPY^{-}$ cells. Adipocyte colonies (CFU-As) were defined as $Hoechst^{+}BODIPY^{+}$ population of cells, characterized phenotypically by the formation of mature lipid droplets, and lacking any apparent Alizarin red S staining (Fig. 3.1b). The remaining colonies (CFU-AO) were determined to be multilineage colonies positive for Hoechst and displayed a

mixture of more than one colony type marker, i.e. Hoechst^{+}BODIPY+ve with some Alizarin red S staining (Fig. 3.1b).

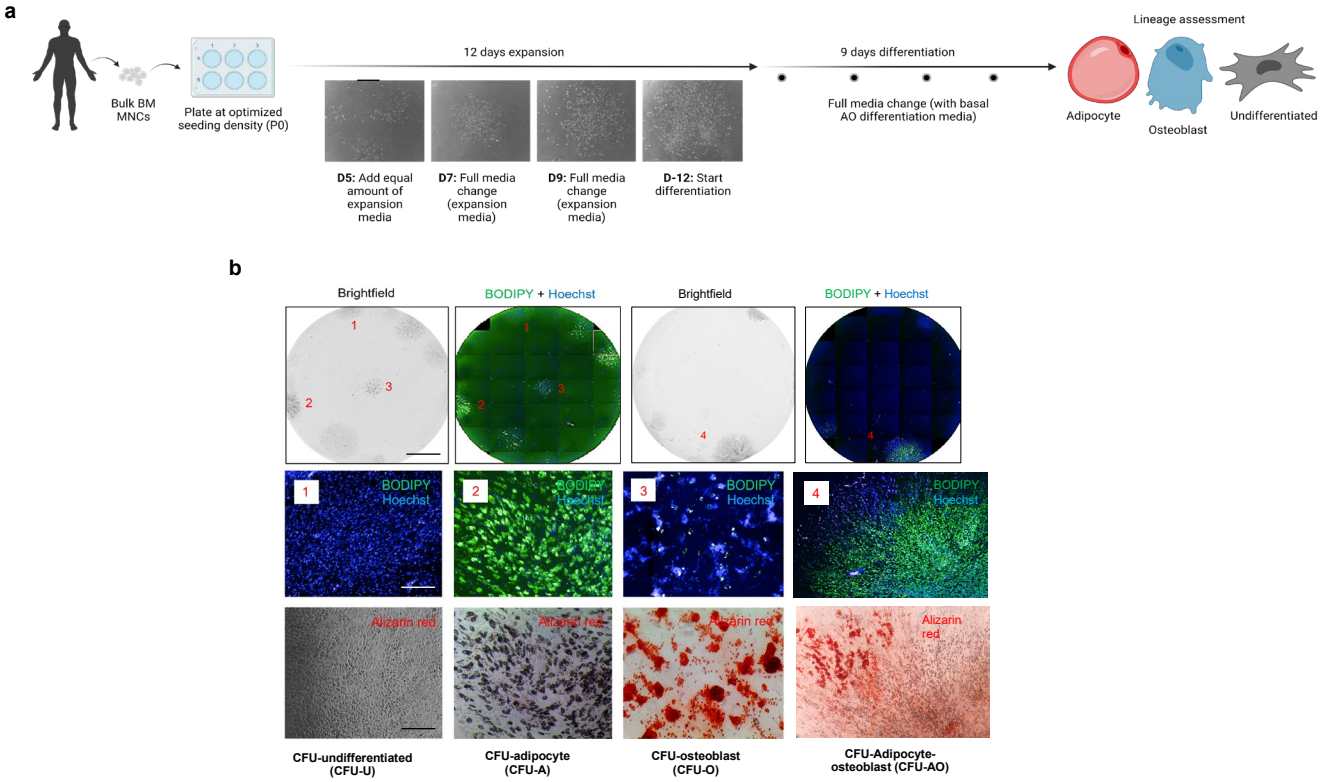

Figure 3.1: Development of an *in vitro* mesenchymal CFU assay. (**a**) Overview of mesenchymal CFU assay. Bulk BM-MNCs were seeded at an optimum density into a 6 well-plate. Culture was expanded for 12 days (brightfield images showing formation of colony outgrowth, scale bar 300 µm) before differentiation was initiated in a basal medium permissive for both osteoblast and adipocyte differentiation for a total of 9 days. At day 21, colonies were stained with BODIPY and Alizarin red to evaluate the fate choice of each progenitor. (**b**, top row) Representative wells illustrating the different colony types from AML patient #1. Brightfield images display all colonies present in each well (CFU-U, CFU-A, CFU-O, CFU-AO). (**b**, middle row) Fluorescent and (**b**, bottom row) colour brightfield images of each mesenchymal progenitor type, scale bars 450 µm.

3.1.2 Change in mesenchymal progenitor composition upon prolonged in vitro culturing

Despite the obvious remodeling of the niche upon expansion of the leukemic disease in the marrow, reports regarding which mesenchymal population is implicated in AML remain

controversial and vary across different studies. To elucidate this discrepancy observed in the field, we investigated the behaviour of MSCs in by performing mesenchymal CFU assay on BM-MNCs from AML patients as well as healthy donors at initial plating (passage 0), and then comparing the progenitor output to BM-MSC lines derived from these same samples but at a later passage (Fig. 3.2a). For the later passage samples, a limiting dilution assay (LDA) was done from the bulk MSC lines in order to capture the progenitor compartment (Supplemental Fig. 3.2a). Interestingly, we saw a change in the progenitor readout for all the samples assessed upon prolonged *in vitro* culturing, whether it be healthy or AML, depicting the selection of certain mesenchymal progenitors in a stochastic manner (Fig. 3.2b). If we assume an adipocyte-osteoblast progenitor can give rise to both adipocytic and osteoblastic populations equally, we can likewise calculate the overall adipogenesis and osteoblastogenesis potential of each sample, denoted as % adipo potential (derived by combining the proportion of CFU-A and half of the proportion of CFU-AO) and % osteo potential (derived by combining the proportion of CFU-O and half of the proportion of CFU-AO). Only 1 AML sample appeared to show reduction in their overall adipogenesis potential, while both samples showed an increase in their osteoblast capacity at a later passage (Fig. 3.2c). On the other hand, the 2 healthy lines interrogated showed opposite results. Wherein Healthy 7 exhibited a marked decrease in its osteoblastic differentiation and relatively similar levels of adipogenesis capacity upon prolonged culturing, Healthy 1 displayed higher osteoblast potential and a dramatic decrease in its adipocyte capacity at a later passage (Fig. 3.2c). As such, depending on which healthy samples were used as a normal reference and the passage number at which the mesenchymal samples were assessed, the interpretation regarding which mesenchymal entity is impaired might differ, recapitulating the discrepancies that are often observed in the field.

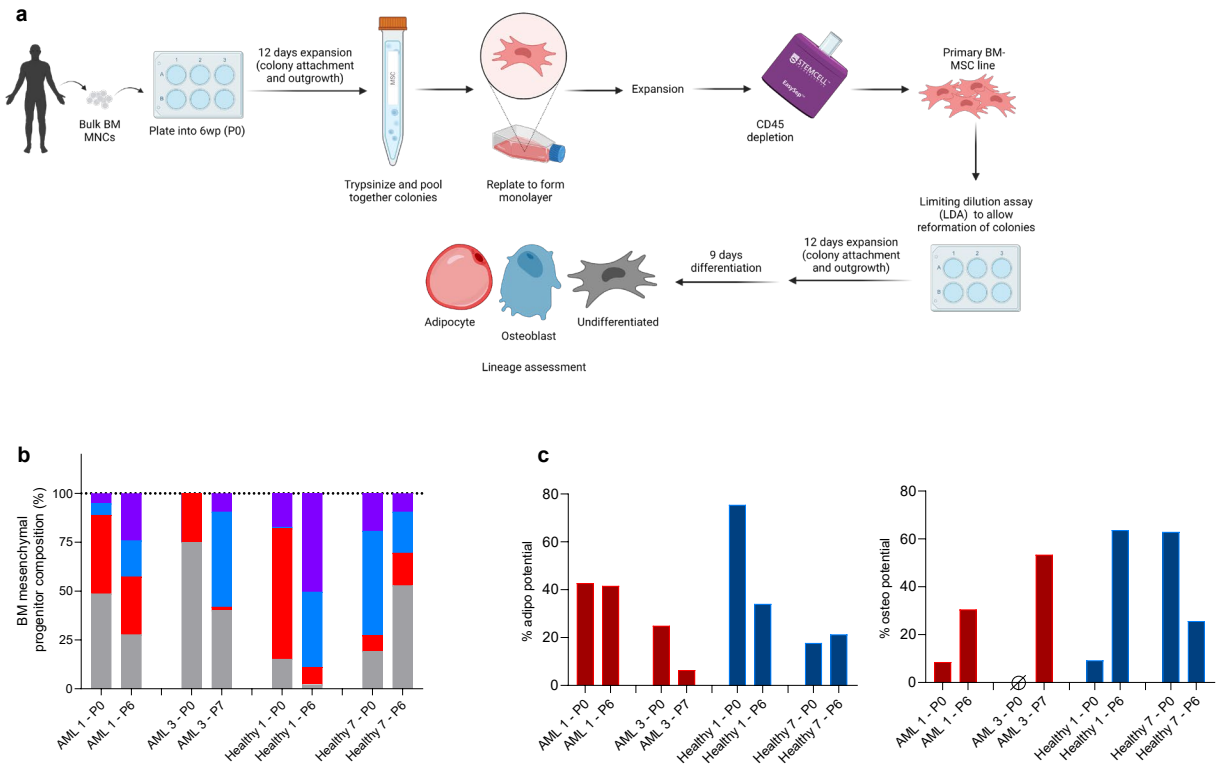

Figure 3.2: Mesenchymal CFU assay on later passage BM-MSCs show change in progenitor composition from initial plating. (**a**) Schematic of experiment. BM-MNCs were seeded into a 6wp to allow for stromal cell adherence. Following colony expansion at day 12, cells were either differentiated for the mesenchymal CFU assay (Fig. 1a) or trypsinized and replated into a flask to allow for monolayer formation of MSCs. The monolayer was expanded until enough cells were collected for CD45 depletion, such that only a pure mesenchymal population remains. The cells, now called a primary BM-MSC line, were cultured over several passages, before they were then replated into a 6wp at very low seeding densities (in a LDA assay) to enable colony-forming unit (CFU) formation. After 12 days of expansion, the colonies were exposed to a basal adipocyte-osteoblast differentiation medium for 9 days, before their fate choices were assessed. (**b**) Composition and (**c**) overall adipogenesis (left) and osteoblastogenesis (right) potential of mesenchymal progenitors for AML and healthy samples at initial plating (P0) compared to later passages (P6 for AML 1 and Healthy 1 and 7, P7 for AML 3). *n*=15 technical replicates/well for AML 1 and 3 P0, *n*=18 for AML 3 P7, Healthy 1 P0, Healthy 7 P0 and P6, *n*=10 for AML 1 P6, *n*=9 for Healthy 1 P6. Data are shown as stacked means (**b**) or bars (**c**).

3.1.3 Construction of a mesenchymal lineage tree

Mesenchymal stem cells not only display inter- and intra-donor heterogeneity (Bianco et al. 2013; Bianco, Robey, and Simmons 2008), but they are also very vulnerable to the slightest

changes in their culturing environment (Leuven 2011; Sisakhtnezhad, Alimoradi, and Akrami 2017). To investigate whether the change in progenitor composition we observed earlier stems from a Darwinian selection of certain mesenchymal clones as a result of continuous *in vitro* culturing, we tracked the fate choice of each mesenchymal colony and constructed a mesenchymal lineage tree from the colonies we isolated. Following plating of bulk BM-MNCs to plastic surface, we transferred each colony outgrowth to a single well of a 96-wp before the colony was split into 2 identical wells (Fig. 3.3a). This allows for their differentiation potential to be assessed as they are expanded over multiple passages until the population ceases to proliferate. Unexpectedly, we not only observed the selection of certain mesenchymal clones, but it appeared that not a single clone retained their initial mesenchymal identity (Fig. 3.3b). While some colonies stayed true to their lineage choice for a few passages, they were still subject to a substantial number of lineage transitions, and this was seen in both healthy and AML lines tested (Fig. 3.3b). Despite the varying degrees of transition that occurred between passages, all clones displayed a trend towards the osteoblast lineage (Fig. 3.3b), which is reminiscent of the finding from an earlier study (Wolock et al. 2019).

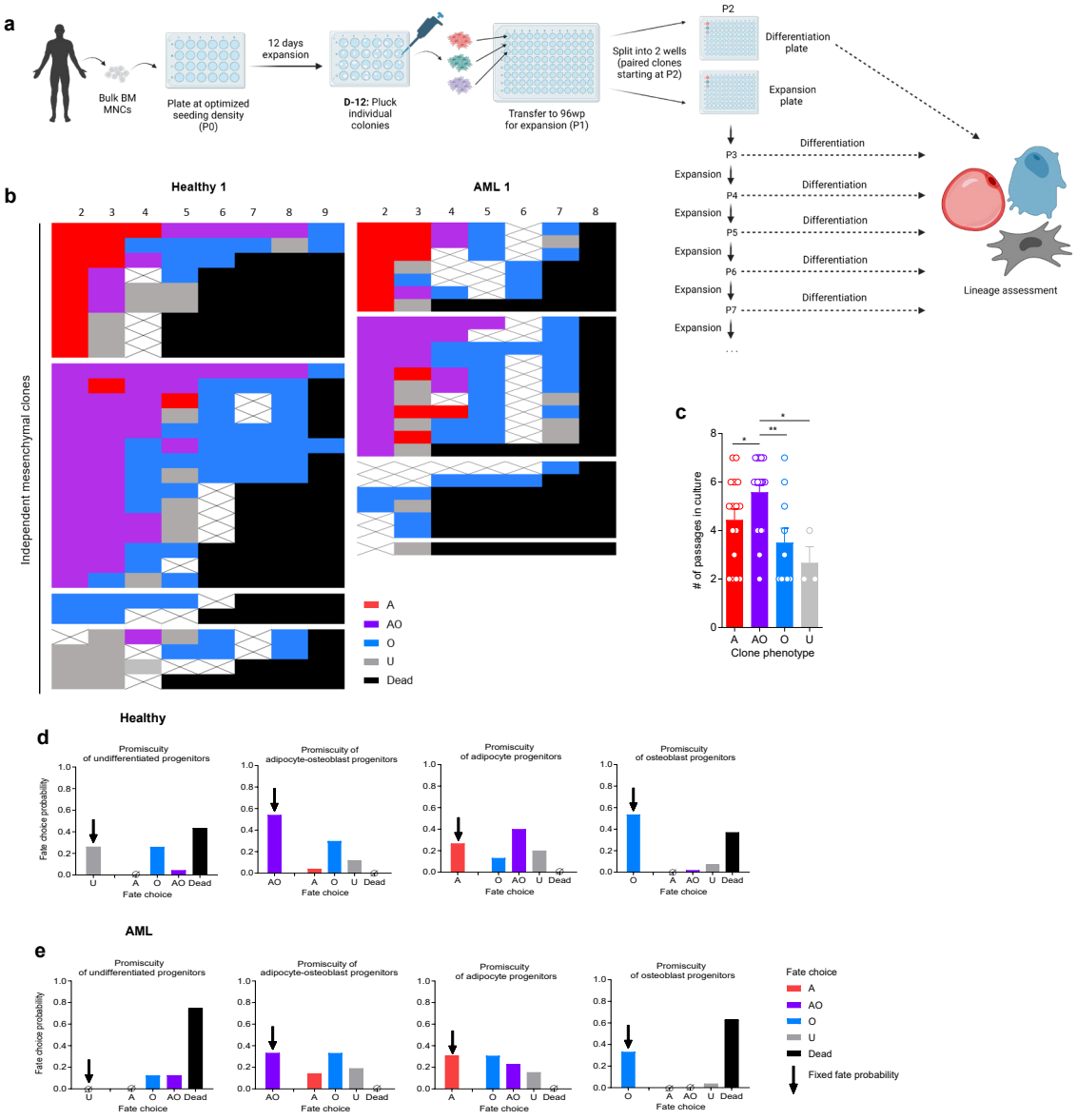

Figure 3.3: BM mesenchymal progenitors are plastic and display a tendency to drift towards the osteoblast lineage over passages in culture. (**a**) Schematic for (**b**) lineage tracking of bone marrow mesenchymal colonies from a healthy individual and an AML patient over multiple passages (*N*=31 independent colonies for Healthy 1, *N*=25 for AML 1). Each row represents an individual colony, and each column denotes the fate choice of the colony at a particular passage. Hashed colonies indicate there were not enough cells for differentiation to determine the fate choice of the colony at that passage. (**c**) Lifespan of each mesenchymal progenitor in culture. (**d**) Fate choice probability of mesenchymal progenitors from healthy compared to (**e**) AML patients, showing the probability of each mesenchymal progenitor to stay true to their initial fate choice (denoted by the black arrow, fixed fate probability) or their probability to transition into other mesenchymal phenotypes. Data are shown as means ± s.e.m (**c**) or bars (**d**, **e**). Statistical significance was assessed by unpaired *t*-test (**c**).

3.1.4 Mesenchymal progenitors show varying degrees of self-renewing capacities

Whether the transitions observed point to the plastic nature of MSCs themselves, or whether this phenomenon is simply a product of intra-heterogeneity that exists within each MSC colony i.e., varying degrees of stem and progenitor population in a single colony undergoing asymmetrical self-renewal, remains to be determined. It was apparent, however, that CFU-AO possessed the highest degree of self-renewing capacity and was the mesenchymal progenitor that was also most devoted to their initial fate choice along with CFU-O (Fig. 3.3c). CFU-A appeared to be more promiscuous and often transitioned into a CFU-AO before eventually choosing the fate of an osteoprogenitor (Fig. 3.3d, e). Interestingly, we did not observe the opposite, i.e. a CFU-O transitioning into a CFU-AO before going on to choose an adipocytic fate, suggesting that the osteoblast lineage appears to be the end-point of mesenchymal clones during *in vitro* propagation. While the number of CFU-U we isolated was scarce, we could see that they had the lowest self-renewing capacity and often immediately ceased to proliferate after a few passages in culture (Fig. 3.3c). This was also true for clones that initially were of other phenotypes, but eventually transitioned into a CFU-U, indicating that the CFU-U phenotype perhaps represent a subset of mesenchymal clones that are undergoing senescence or impaired in their proliferative capacity. Overall, however, the lineage transition probability of each mesenchymal clone did not seem to be particularly different between healthy and AML mesenchymal populations (Fig. 3.3d, e). Thus, we propose an alternative paradigm for the mesenchymal hierarchy, where instead of a one-directional, stereotypical pyramid hierarchy, lineage-committed mesenchymal progenitors (CFU-AO, CFU-A, CFU-O) exist on an equal plane, each displaying promiscuity of varying levels towards other mesenchymal phenotypes (Fig. 3.4). CFU-Us, which show the least capability to

self-renew, are situated on a different plane as a progenitor with this phenotype will most likely cease to proliferate soon after they are introduced in culture (Fig. 3.4).

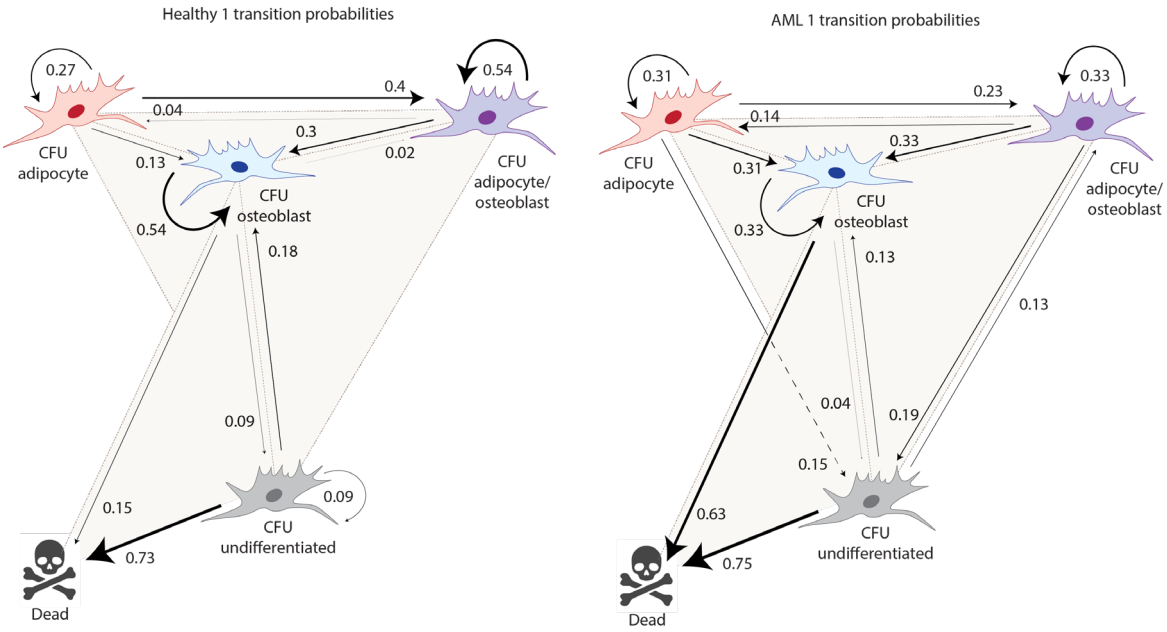

Figure 3.4: Undifferentiated mesenchymal progenitors exist at the bottom of the mesenchymal hierarchy and show the least proliferative capability. Putative hierarchy of the mesenchymal compartment in healthy (left) and AML diseased state (right) based on their self-renewing and fate choice probability. Arrow thickness denotes probability; straight arrows represent the probability of a mesenchymal progenitor to transition into a different phenotype, while curved arrows refer to the self-renewing probability/fixed fate choice of a progenitor.

In conclusion, BM-MSCs show unexpected plasticity upon prolonged period of culturing, which could change their clonal composition at time of assessment compared to when they are first isolated from donors. This phenomenon is observed in both AML and healthy BM-MSC samples, and perhaps contribute to the disparity seen in the field with regards to the impairment in differentiation potential of AML BM mesenchymal cells.

3.2 BM-MSCs from AML patients are enriched in undifferentiated progenitors, exhibit reduced self-renewing and proliferative capacity, and undergo early senescence *in vitro*

3.2.1 Accumulation of undifferentiated mesenchymal progenitors in AML patients

A total of 11 AML and 8 healthy BM samples were interrogated for their progenitor capacity using the mesenchymal CFU assay. All AML samples were drawn at diagnosis, and both AML and healthy samples were derived from donors of varying ages (Table 1, 2).

Although at differing levels, AML BM-MSCs showed lower number of all types of mesenchymal progenitors compared to BM-MSCs from healthy donors (Fig. 3.5a, b). Comparing the fold reduction of each mesenchymal progenitor type, it seemed that mature, lineage-committed progenitors (CFU-AO, CFU-A, CFU-O) were more implicated by the presence of the leukemic disease than the undifferentiated population (Fig. 3.5c). While there did not appear to be any difference in the overall adipogenesis and osteoblastogenesis potential between AML and healthy BM-MSCs (Fig. 3.5d), seen also from the relatively similar proportions of CFU-AO, CFU-A, and CFU-O (Fig. 3.5e), it stood to be true that the total proportion of these mature, lineage-restricted progenitors were lower in samples derived from AML patients, while healthy BM-MSCs demonstrated the opposite pattern, with lineage-committed progenitors being the major population observed (Fig. 3.5f). In addition, we observed an increased proportion of the undifferentiated progenitor compartment in AML patients (Fig. 3.5e, f) which reflected the lower fold reduction in CFU-U population compared to other mature, lineage-restricted mesenchymal progenitors (Fig. 3.5c).

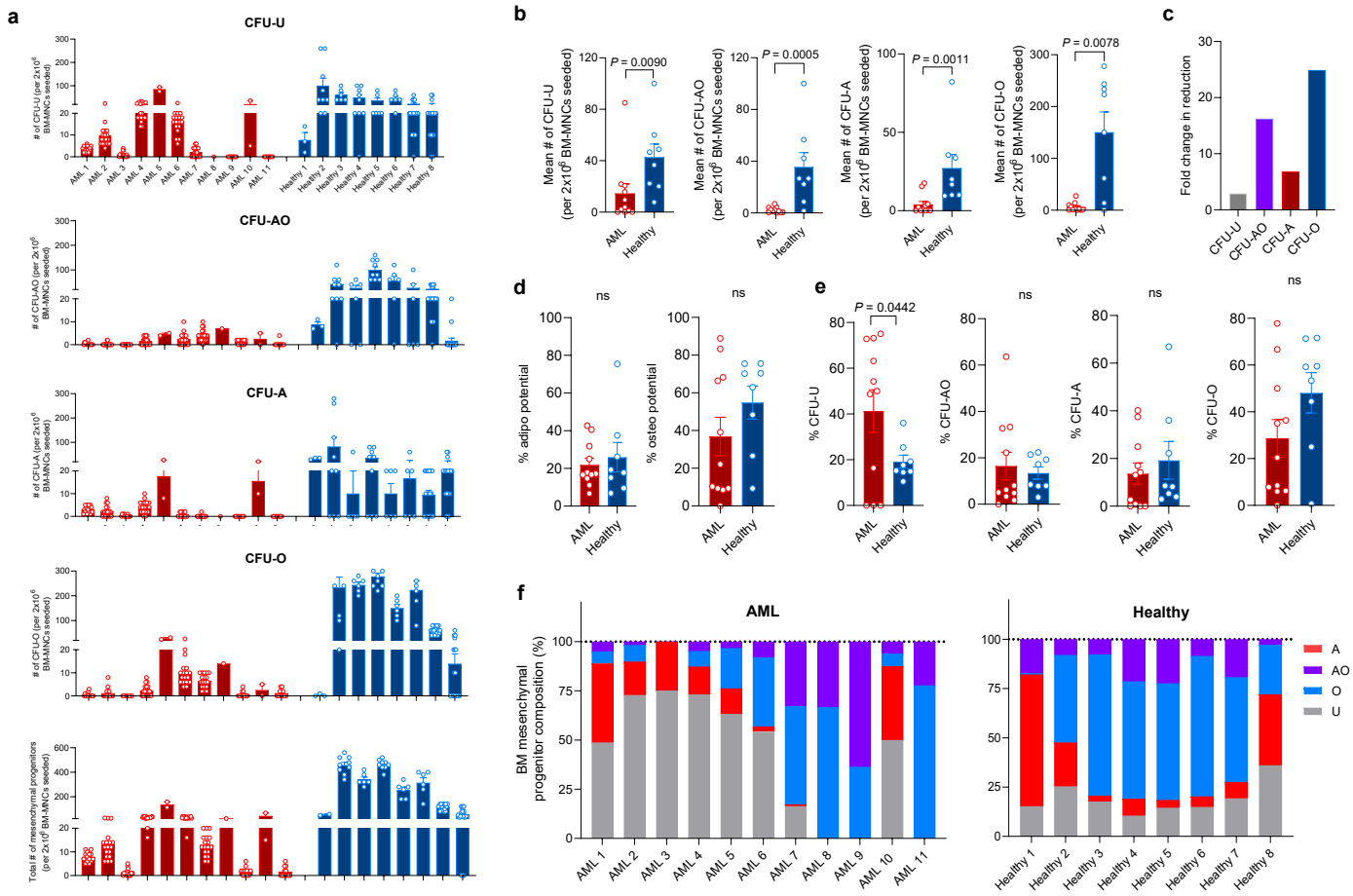

Figure 3.5: AML BM-MSCs are enriched for undifferentiated mesenchymal progenitors. (**a**) Number of mesenchymal progenitors in BM-MSCs derived from AML patients (red) in comparison to healthy donors (blue). Data points represent individual CFU wells. *n*=15 independent wells/technical replicates for AML 1, 3, *n*=18 for AML 2, 4, 6, 7 *n*=2 for AML 5, 10, *n*=1 for AML 8, *n*=12 for AML 9, 11; *n*=6 independent wells/technical replicates for Healthy 2, 3, 5, 6, *n*=9 for Healthy 4, *n*=18 for Healthy 7 and 8, *n*=3 for Healthy 1. (**b**) The average number of each mesenchymal progenitor type in AML and healthy BM-MSCs. Each point represents an individual patient/donor; *N*=11 AML patients, *N*=8 healthy donors. (**c**) Fold change reduction of each mesenchymal progenitor type (healthy to AML). (**d**) Overall adipogenesis and osteoblastogenesis potential as well as (**e**) proportion of undifferentiated (CFU-U), adipocyte-osteoblast (CFU-AO), adipocyte (CFU-A), and osteoblast progenitors (CFU-O) of BM-MSCs from AML patients and healthy donors (*N*=11 samples for AML, *N*=8 samples for Healthy). (**f**) Composition of mesenchymal progenitors in BM-MSCs derived from AML patients (left) in comparison to healthy donors (right). Data are shown as means ± s.e.m (**a**, **b**, **d**, **e**), stacked means (**f**), or bars (**c**). Statistical significance was assessed by unpaired *t*-test (**d**, **e**), Mann-Whitney test (**b** for CFU-U**,** AO, and A), and Welch's *t*-test (**b** for CFU-O).

3.2.2 Impaired proliferative and self-renewing capacity of AML BM-MSCs

The impairment of AML BM-MSCs likewise appear to extend beyond their ability to differentiate into functional mesenchymal cells. AML blasts have been found previously to induce a pro-tumoral environment in the BM which leads to stromal cell senescence (Abdul-aziz et al. 2019). To investigate whether this characteristic of AML stroma can be recapitulated *in vitro*, we isolated MSCs from primary AML and healthy BM samples, and noted the doubling time of each BM-MSC line as they were propagated *in vitro*. The majority of BM-MSCs isolated from AML samples were found to be remarkably difficult to expand, and this was illustrated from their longer doubling time compared to healthy BM-MSCs (Fig. 3.6a). AML 2 and 14 even experienced negative doubling times at their latest passage (passage 5) due to the number of cells collected being lower than the number of cells initially plated, which suggests that the population is dying (Fig. 3.6a). We also performed a limiting dilution assay (LDA) on AML and healthy BM-MSCs at later passages and saw that AML BM-MSCs possessed lower frequency of cells capable of forming colony outgrowth (CFU-F) compared to healthy BM-MSCs (Fig. 3.6b). To further elucidate this disparity in proliferation and self-renewal, we performed a senescence-associated β-galactosidase (SA-β-gal) staining of AML BM-MSC samples in comparison to a healthy BM-MSC line which has been propagated for a similar length of time in culture. AML BM-MSCs were found to exhibit higher β-galactosidase activity that is associated with senescence *in vitro*, while MSCs derived from a healthy donor at the same passage number showed lower amount of such activity and had low β-galactosidase staining, indicating that AML BM-MSCs have a larger proportion of senescing cells in comparison to healthy BM-MSCs (Fig. 3.6c, d).

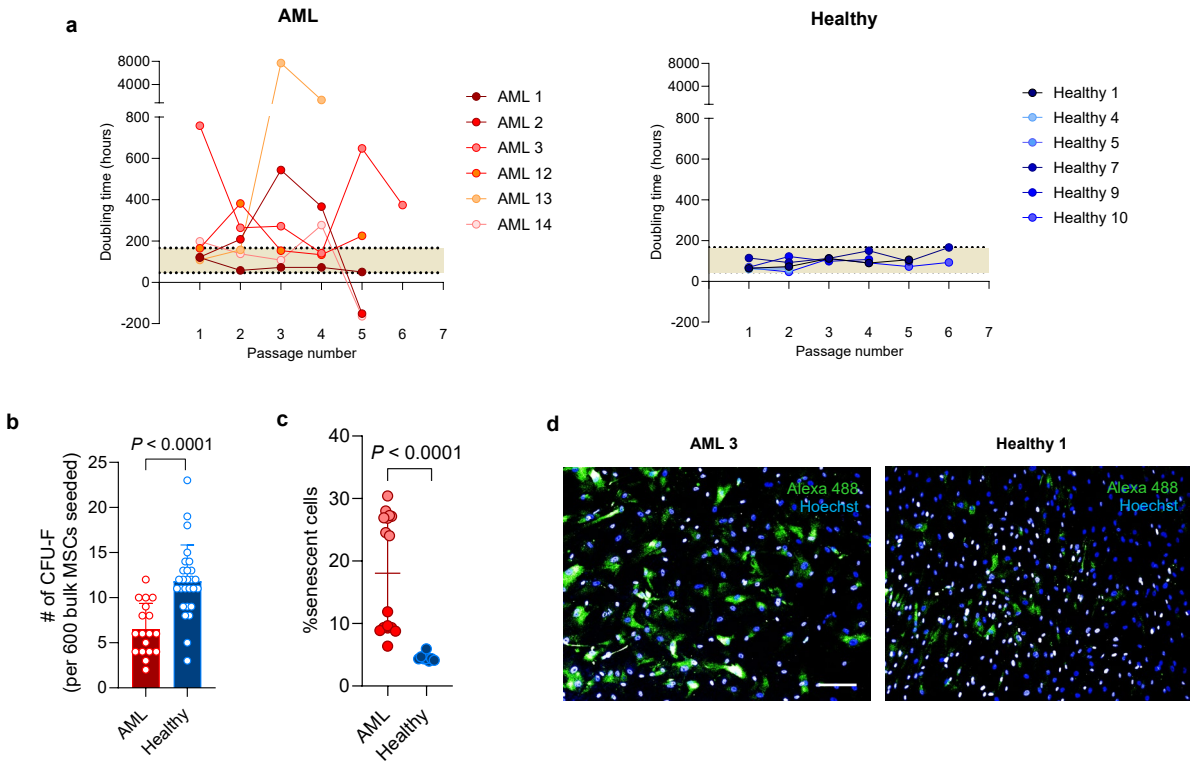

Figure 3.6: BM-MSCs from AML patients have reduced self-renewing capacity and show early senescence *in vitro*. (**a**) Population doubling times of BM-MSC lines from AML patients (represented in shades of red) and healthy donors (represented in shades of blue) during *in vitro* expansion from passage 1 to passage 6 (*N*=6 for AML lines and *N*=6 for healthy lines). The coloured area in beige represents the population doubling time occupied by healthy BM-MSC lines. (**b**) Frequency of mesenchymal cells capable of forming colony outgrowth for every 600 mesenchymal cells seeded in culture (AML 3, *n*=18 technical replicates/wells; Healthy 6 and 7, *n*=27 pooled from *N*=2 independent samples). (**c**) Percentage of BM-MSCs from AML patients (AML 3 and 12, passage 7 and 6 respectively, *n*=8 for each sample) and a healthy donor (Healthy 7 at passage 6, *n*=8) showing senescence-associated β-galactosidase (SA-β-gal) activity. (**d**) SA-β-gal staining of BM-MSCs from an AML patient (AML 3, left) compared to a healthy donor (Healthy 1, right). Live cells are stained with Hoechst (blue) while senescence staining is shown in green. Scale bar, 500 µm. Data are shown as means ± s.e.m (**b**, **c**) or scattered dot plot (**a**). Statistical significance was assessed by unpaired *t*-test (**b**) or Mann-Whitney test (**c**).

Collectively, our findings suggest that the differentiation capacity of AML BM-MSCs is impaired, with the disease preferentially sparing the undifferentiated mesenchymal population while equally compromising adipocyte and osteoblast progenitors (Fig. 3.5). In addition, AML BM-MSCs seem to have a shortened cellular lifespan and demonstrate both attenuated proliferative and self-renewing capacity (Fig. 3.6). It is worth noting that this remodeling of the

stroma into a pro-tumoral senescent phenotype is sustained *in vitro*, even in the absence of leukemic blasts.

3.3 BM-MSCs of relapsed AML patients show heightened osteoblast activity

3.3.1 Increased osteoblastic potential in BM-MSCs from relapsed AML patients

While the dynamics of how niche cells interact with leukemic cells and other BM-resident cells are still not fully understood, we hypothesized that the BM niche, and by extension mesenchymal cells, contain footprints left behind by the disease that would distinguish patients in remission versus those who relapsed that we can incorporate as a part of our current disease monitoring strategies. To do this, we conducted mesenchymal CFU assay on primary AML patient samples throughout their disease progression, selecting samples from patients that managed to achieve remission compared to those that eventually underwent relapse. At first glance, the mesenchymal progenitor composition across each patient sample did not seem to reveal much trend (Fig. 3.7a); however, when we consolidated their overall adipogenesis and osteoblastogenesis potential as well as looked at each mesenchymal progenitor compartment, we saw that the mesenchymal population of patients who relapsed displayed a strong tendency towards the osteoblast lineage (Fig. 3.7b). While this increase was not very pronounced at the early stages of the disease i.e. at diagnosis and following therapy, this increase in osteoblast potential was particularly dramatic in patients undergoing relapse when compared to those that were in remission (Fig. 3.7b, e, g). This trend of increasing osteoblastic activity in relapsed patients was accompanied by the decreased proportion of both undifferentiated (Fig. 3.7c, h) and adipocyte progenitors (Fig. 3.7f, i) as well as an increase in the adipocyte-osteoblast progenitor compartment (Fig. 3.7d, j), which showed a particular skewing towards osteoblast formation (Fig. 3.7k). While

the decrease in undifferentiated progenitor was similar to the osteoblast compartment in that it only became apparent at the time of relapse, the decrease in adipocyte progenitors of relapsed patients could be seen even in samples when disease relapse had not yet been detected in these patients using methods currently used in the clinic (Fig. 3.7i).

Altogether, these observations suggest an underlying mechanism of AML relapse that gears mesenchymal cells towards osteoblast differentiation, the significance of which is yet to be determined, and that perhaps a change in the mesenchymal progenitor composition of patients can be used as an additional parameter when assessing disease regeneration.

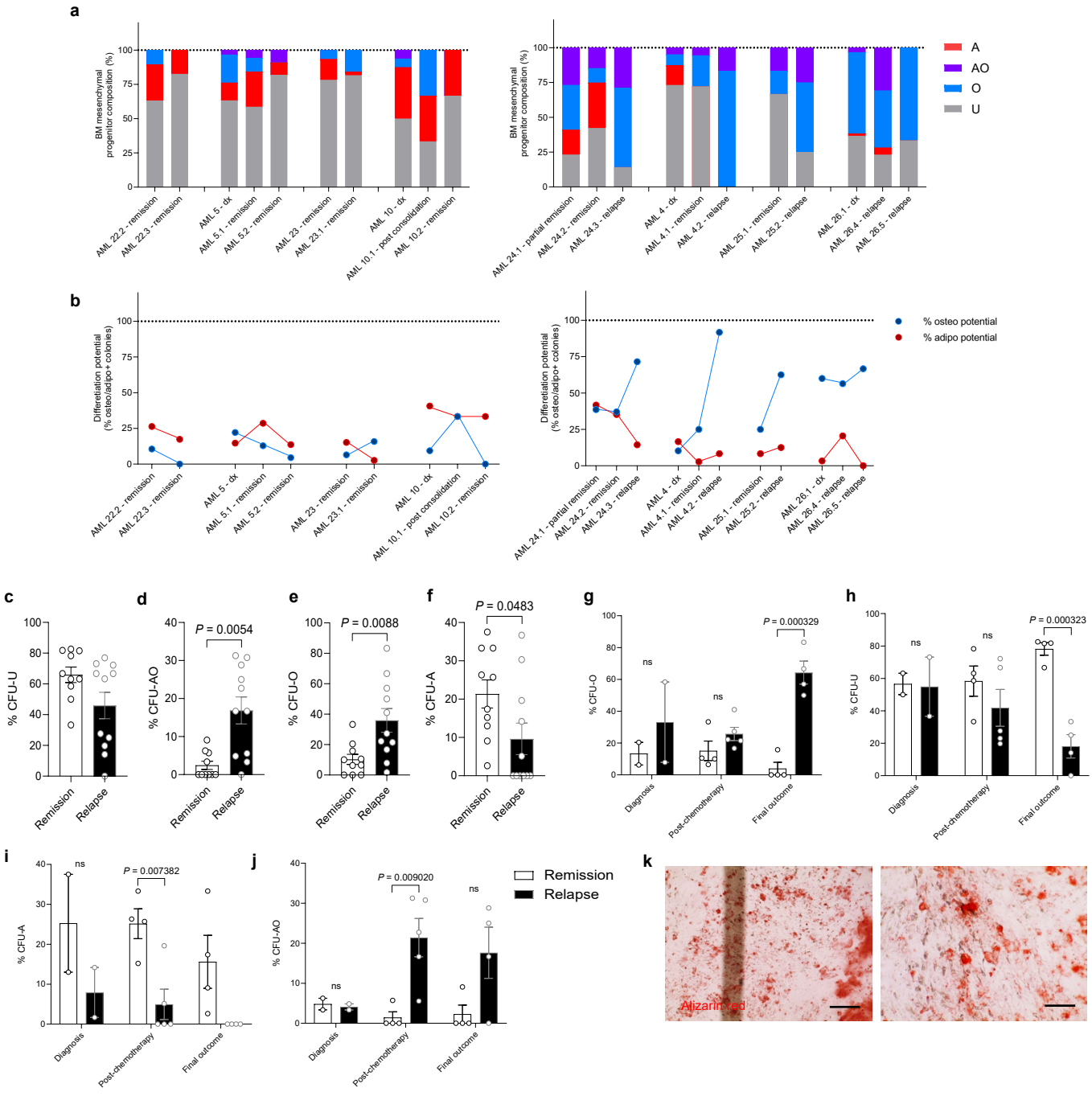

Figure: 3.7 BM-MSCs from relapsed AML patients show increased osteoblast potential. (**a**) Composition of mesenchymal progenitors in BM-MSCs derived from AML patients throughout their disease progression. Patients listed eventually achieved remission status (left; *n*=2 technical replicates for AML 22-2 and 22-3, 5, 5-1, 5-2, 23-1, 10, 10-1, 10-2, *n*=3 for AML 23), or eventually relapsed (right; *n*=3 technical replicates for 24-1, 25-1, 26-4, *n*=5 for AML 24-2 , *n*=6 for 24-3, 26-1, *n*=4 for AML 4-2, *n*=2 for 25-2, 26-5, *n*=1 for AML 4-1, *n*=18 for AML 4). (**b**) Tracking the

adipogenesis and osteoblastogenesis potential of BM-MSCs from patients who managed to achieve remission (left) versus those who relapsed (right). (**c**-**f**) Proportion of each mesenchymal progenitor compartment throughout disease progression for remission versus relapse groups. *N*=2 diagnosis samples for each remission and relapse group; *N*=4 follow-up samples for remission and *N*=5 follow-up samples for relapse group; *N*=4 samples from patients with remission as a final outcome and *N*=5 samples from patients with relapse as a final outcome. (**g**-**j**) Proportion of each mesenchymal progenitor in samples pooled together from remission (*N*=10) and relapse (*N*=11) groups. (**k**) Representative colour brightfield images of a CFU-AO from a relapsed AML (AML 24.3). Calcium mineralization indicating osteoblastogenesis shown in red through Alizarin red staining. Scale bars, 500 μm. Data are shown as stacked means (**a**), dot plot (**b**), or means ± s.e.m (**c**-**j**). Statistical significance was assessed by unpaired *t*-test (**c**-**j**).

3.4 Some factor(s) in the AML sera impairs the differentiation potential of BM-MSCs

3.4.1 AML sera alter fate choice of healthy mesenchymal progenitors

Although the reduced differentiation capacity of AML BM-MSCs appear to be inherent, we were also interested in investigating the role the environment plays in shaping their function and behaviour i.e. whether extrinsic factors such as the serum plays a role in regulating the function and behaviour of the niche. To do this, we seeded BM-MNCs onto a plastic surface and plucked individual colonies into 96 well-plates for expansion. Following the first passage, each colony was split into 2 identical wells (paired seeding) and we exposed them to differentiation medium supplemented with either healthy human serum or serum derived from an AML patient. At the endpoint of the assay, their fate choice was assessed using Alizarin Red (for detection of osteoblastic colonies) and BODIPY staining (for identification of adipocytic colonies) (Fig. 3.8a). We have performed this experiment on 31 independent mesenchymal colonies from a healthy and AML sample using 2 unique healthy and AML sera. Clones differentiated in AML sera displayed a higher number of undifferentiated population compared to those differentiated in healthy sera, with many showing a loss of differentiation capacity (Fig. 3.8b). For example, clone 4, encapsulated by the box in red, initially showed an adipocyte-osteoblast phenotype when differentiated in healthy serum. However when differentiation was done with AML serum, the

clone transitioned into an adipocyte phenotype, indicating a loss of osteoblast potential (Fig. 3.8b, d). In addition, quantification of each paired clones' adipogenesis activity through BODIPY staining revealed lower adipogenesis output for most clones differentiated in AML sera compared to their paired counterparts differentiated in healthy sera (Fig. 3.8c).

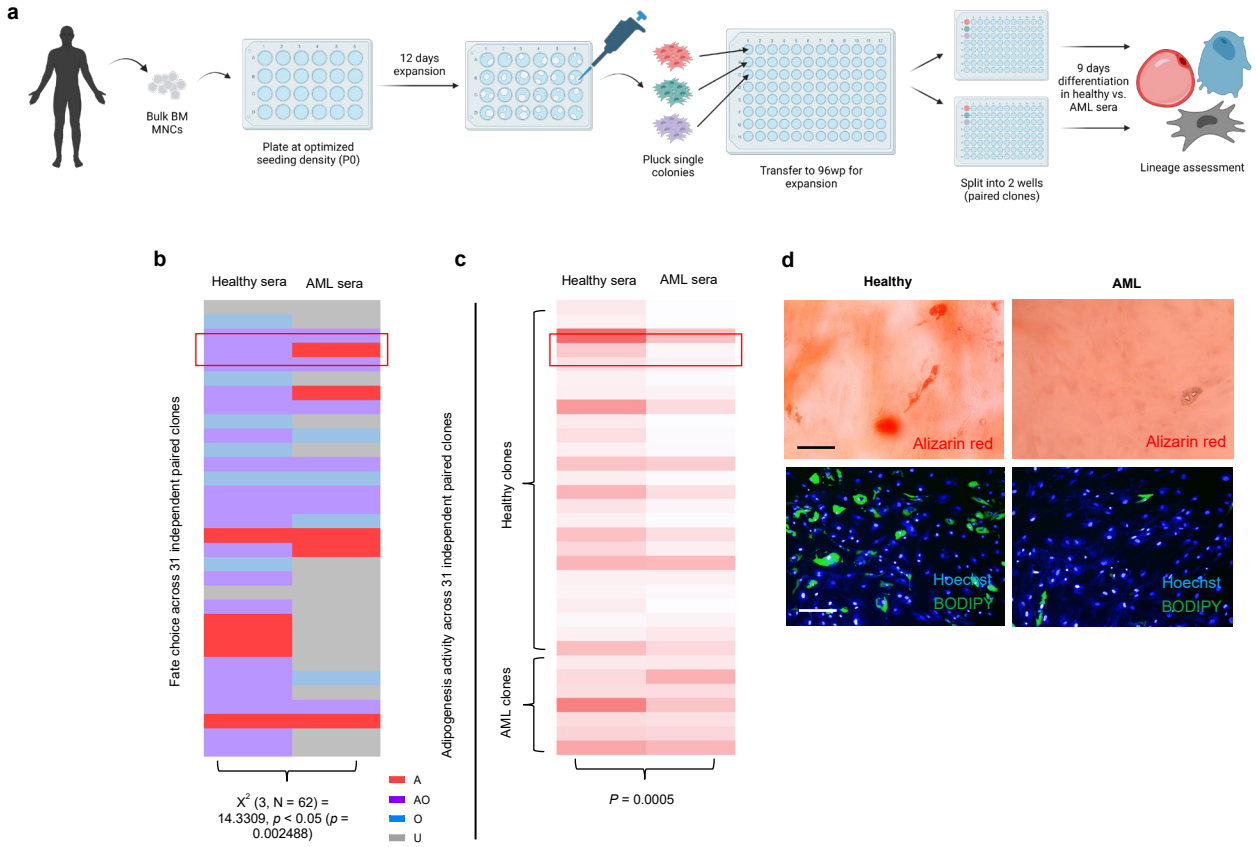

Figure 3.8: AML sera induce a loss of differentiation capacity in mesenchymal progenitors. (**a**) Schematic of experiment. BM-MNCs were seeded onto a plastic surface (passage 0), and colonies were plucked before transferred into a 96-wp for expansion (passage 1). Following the first passage, the colonies were split into 2 identical wells (passage 2) for differentiation in either healthy serum or serum derived from an AML patient. After 9 days, their fate choice was assessed using Alizarin Red and BODIPY staining. (**b**) Fate choice and (**c**) adipogenesis activity of 24 paired colonies from Healthy 1 (pooled from *N*=2 independent experiments) and 7 paired colonies from AML 1 (*N*=1). Clones were differentiated in AML sera (*N*=2, AML 15 and 16) or using sera from healthy donors (*N*=2, Healthy 11 and 12). (**d, top**) Brightfield image showing Alizarin red staining of clone 4 (encapsulated in red box, **b-c**) differentiated in healthy (left) compared to AML serum (right). (**d**, **bottom**) BODIPY staining of clone 4, differentiated in healthy (left) versus AML (right) serum. Live cells are shown through Hoechst staining in blue. Scale bars, 500 µm.

Statistical significance was assessed by chi-square test of independence (**b**, for heatmap showing fate choice) or paired *t*-test (**b,** for heatmap showing adipogenesis activity).

3.4.2 BM-MSCs show impaired adipogenesis capacity in the presence of AML sera

We also assayed primary BM-MSC lines from healthy donors for their differentiation potentials when cultured in the presence of either AML or healthy sera. Sera from all AML patients resulted in suppression of adipogenesis activity, with the exception of AML 18 (Fig. 3.9a). On the other hand, quantification of Alizarin Red staining through absorbance measurement at OD405 showed no particular difference in osteoblastogenesis across all sera conditions tested, except for AML 17, and again AML 18, which showed a particularly high Alizarin red activity (Fig. 3.9b).

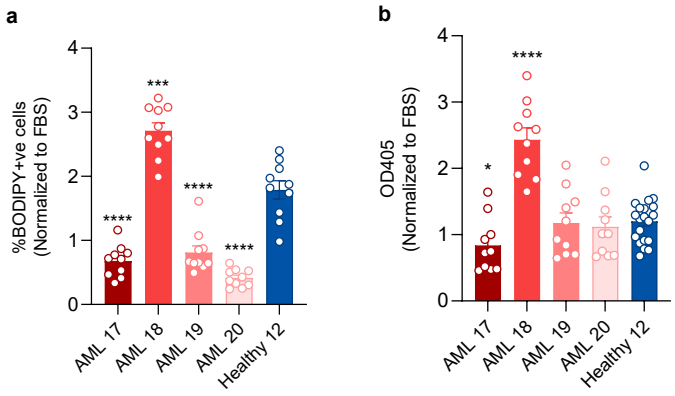

Figure 3.9: AML sera impair the adipogenesis potential of BM-MSCs. (**a**) Percentage of adipocytes in culture as measured through BODIPY staining (n=10 technical replicates per condition). (**b**) Alizarin red activity as measured through OD405 absorbance (n=10 technical replicates per condition). Each culture condition constitutes differentiation in a unique AML serum. Data are shown as means ± s.e.m (**a**, **b**). Statistical significance was assessed by unpaired *t*-test (**a**, **b**).

3.4.3 AML blasts induce an undifferentiated phenotype in mesenchymal progenitors

We hypothesized that AML blasts are involved in secreting factors into the sera that impair the differentiation potential of mesenchymal cells, and sought to determine whether we can causally show this through an *in vitro* co-culture experiment. To do this, we performed the

mesenchymal CFU assay on one of the healthy samples that we tested previously and exposed these healthy colonies later on to the presence of AML blasts throughout the differentiation period using a Transwell system (Fig. 3.10a). Relative to the colonies that were differentiated without exposure to leukemic blasts, the co-culture condition resulted in the ablation of both adipocyte and adipocyte-osteoblast colonies (Fig. 3.10b, c). When looking at the progenitor composition, it appeared that the addition of leukemic blasts also elevated the proportion of undifferentiated populations (Fig. 3.10c, e), reiterating our previous observation with regards to the accumulation of undifferentiated mesenchymal progenitors in AML patients seen through both our mesenchymal CFU assay as well as serum experiment (Fig. 3.5 and 3.8). The presence of leukemic cells also seemed to diminish the adipogenesis potential of healthy BM-MSCs, while the osteoblast potential remained relatively unchanged (Fig. 3.10d, e).

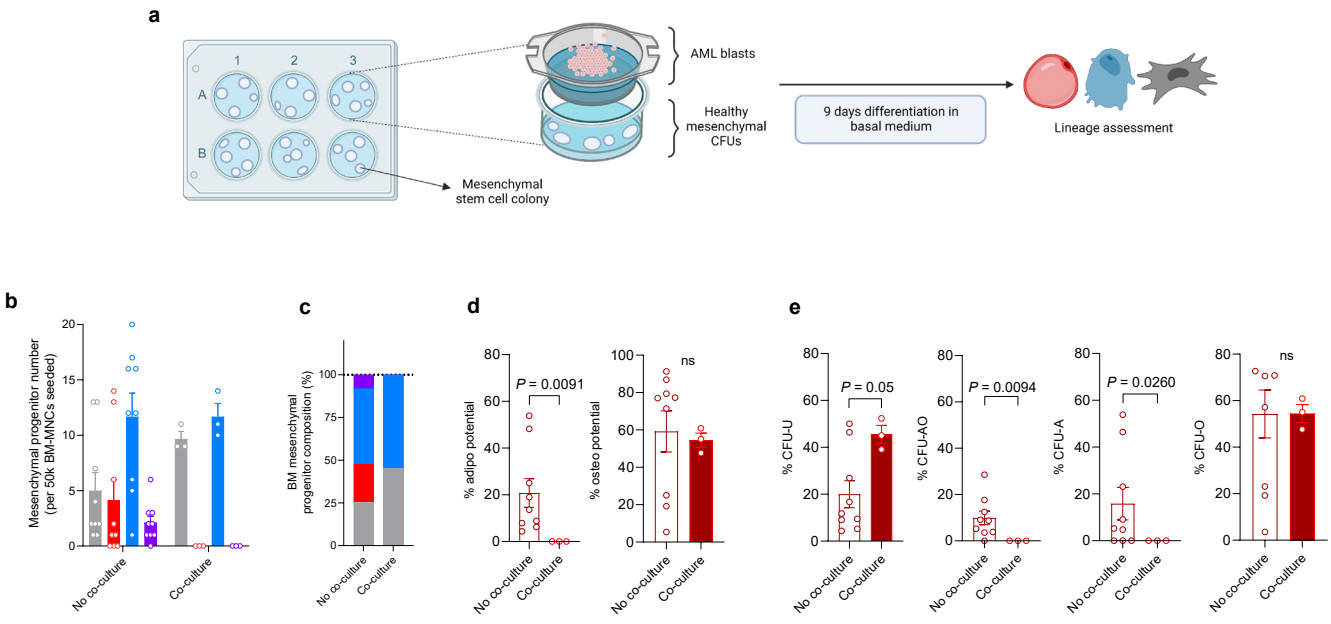

Figure 3.10: Introduction of leukemic blasts in culture attenuates the adipogenesis potential of BM mesenchymal cells. (**a**) Schematic for *in vitro* Transwell co-culture system. AML blasts (AML 21) were added to the upper chamber while healthy mesenchymal CFUs (Healthy 2) were exposed to differentiation medium in the lower chamber. Fate choice of each colony was noted at the end-point of the assay. (**b**) Mesenchymal progenitor number and (**c**) composition of healthy BM-MSCs (Healthy 2) differentiated in the absence or presence of leukemic cells; *n*=9 technical

replicates for the no co-culture condition, *n*=3 technical replicates for the co-culture condition. (**d**) Overall adipogenesis (left) and osteoblastogenesis (right) potential, as well as (**e**) proportion of individual mesenchymal progenitor compartments of MSCs differentiated in isolation or with leukemic blasts. *n*=9 technical replicates for the no co-culture condition, *n*=3 technical replicates for the co-culture condition. Data are shown as means ± s.e.m (**b**, **d**, **e**) or stacked means (**c**). Statistical significance was assessed by unpaired *t*-test (**d**, **e**).

Together, these observations suggest that AML blasts can exert impairment to the differentiation potential of BM-MSCs in a manner that may not require direct physical interaction (i.e. through secretion of some factor(s) into the BM milieu).

3.5 Identification of a novel adipogenesis-inducing molecule through an *in vitro* BM mesenchymal screen

3.5.1 Discovery of an adipogenesis-inducing compound from the Spectrum Library

While we observed an accumulation of undifferentiated mesenchymal progenitors in AML patients (Fig. 3.5), their reduced proliferative capacity makes them unsuitable for use in any high-throughput *in vitro* chemical modulation assays (Fig. 3.3, 3.4). On the other hand, adipocyte populations seem to be the mesenchymal compartment that is consistently impaired in patients throughout the progression of their disease (Fig. 3.5, 3.7-3.10), more so than osteoblast progenitors, whose increased potential might be associated with relapse events in patients (Fig. 3.7). Additionally, we have also shown in a previous study the functional relationship between BM adipocytes and myelo-erythropoiesis, and that rescue of adipogenesis in the marrow helps recover normal erythropoiesis function during an AML diseased state (Boyd et al. 2017). For this reason, we deem adipocytes as the most viable population for therapeutic targeting.

We sought to discover a novel adipogenesis-inducing compound that works independent of PPARγ, the master transcription factor regulating adipogenesis, due to the toxicity issues surrounding PPARγ agonists. To do this, we performed a high-throughput screening of 2560 small molecules from the Spectrum Library on a MSC line, iMSC3, as a primary screen at a single concentration dose (Fig. 3.11a), which has been optimized for and tested for its robustness and promiscuity in picking up false positives (Supplementary Fig. 3.19). From this primary screen, we reported the discovery of 172 molecules which had the capacity to strongly induce adipogenesis. The remaining molecules either did not manage to significantly promote adipogenesis or were shown to have high relative adipogenesis activity but very low cell counts, implying toxicity (Fig. 3.11b). These set of 172 molecules were further tested in a dose-response format on a primary BM-MSC derived from a healthy donor at a 1:2 dilution starting from 10 μM (Fig. 3.11c), and barring any compounds that were already known previously to work through PPARγ, we discovered 11 novel molecules that seemed to promote adipocyte differentiation on BM-MSCs (Fig. 3.11d). As the goal of this screen is to discover a molecule that can eventually be administered into patients, we validated the adipogenesis-inducing activity of these compounds by testing them on another healthy BM-MSC line as well 2 other lines derived from AML patients (Fig. 3.11e). Among these 11 molecules, only 1 molecule, Isoginkgetin, appeared to consistently promote adipogenesis across all the lines assayed, although to a less dramatic extent than our positive control GW1929, which is a well-known PPARγ agonist (Fig. 3.11f). The addition of Isoginkgetin to BM-MSCs *in vitro* seemed to promote adipogenesis that was somewhere in between our empty and positive controls, as observed from both the extent of mature lipid droplets formation (Fig. 3.11g) and the dose-response curves (Fig. 3.11h).

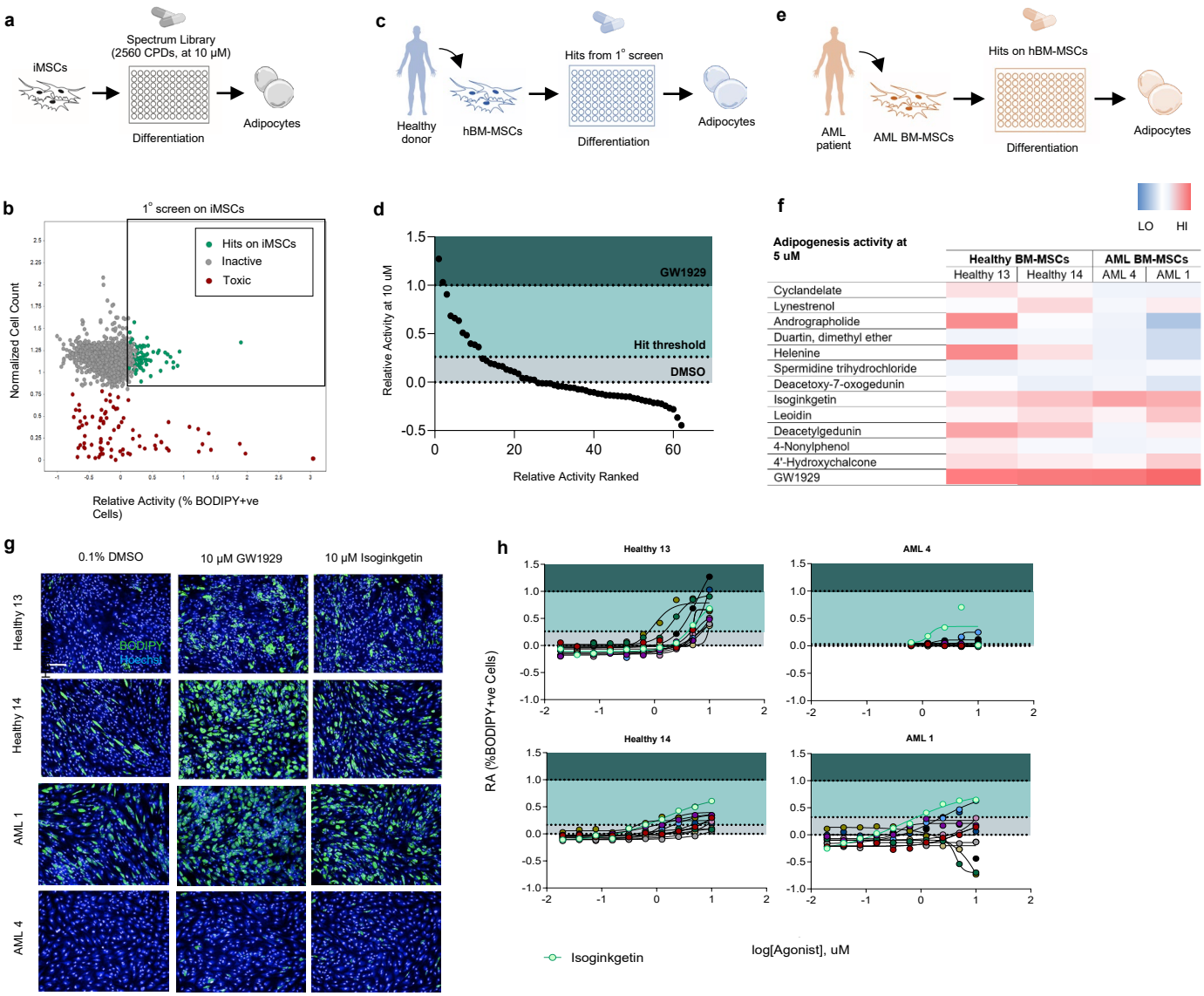

Figure 3.11: Identification a novel adipogenesis-inducing molecule through an *in vitro* BM mesenchymal screen. (**a**) 2,560 compounds from the Spectrum library were screened on Immortalized mesenchymal stem cells (iMSCs) for their adipogenesis-promoting capacity. (**b**) Hit compounds were selected on the basis of adipogenesis-inducing activity (relative activity of %BODIPY+ve cells, x-axis) as well as viability (normalized cell count, y-axis). (**c**) Secondary screen of adipogenesis-promoting compounds (**a**-**b**) on primary BM-MSCs from a healthy donor (Healthy 13). Compounds were tested in a dose-response starting at 10 µM, in a 1:2 dilution. (**d**) Relative activity of compounds at 10 µM were ranked in order to determine hits to be further tested for tertiary screen. (**e**) Tertiary screen of hit compounds from (**c**-**d**) on 2 AML BM-MSCs (AML 1, 4) and another healthy BM-MSC (Healthy 14). (**f**) Heatmap summarizing the adipogenesis-promoting capacity (relative activity of %BODIPY+ve cells) of the hits (**c**-**d**) at 5 µM on all 4 primary BM-MSC lines tested (blue represents low adipogenesis, while red indicates robust adipogenesis activity). (**g**) Fluorescent images of the adipogenesis-initiating capacity of

Isoginkgetin (left) at 10 μM in comparison to empty control (left) and GW1929 (middle) for 4 BM-MSC lines. Blue represents live cells (Hoechst+ve cells) while green shows staining of mature lipid droplets (BODIPY+ve). Scale bar, 300 μm. (**h**) Dose-response curves of molecules shown to act as a promoter of adipogenesis (measured through relative activity) on both primary and secondary screens. 10 concentrations tested for Healthy 13, 14, and AML 1 (*n*=10); 5 concentrations tested for AML 4 (*n*=5). Dose-response was performed in 1:2 dilution starting at 10 μM. All data are shown as scattered dot-plot (**b**, **d**) or dose curves (**h**).

3.5.2 Isoginkgetin works independently of PPARγ

Isoginkgetin is a novel compound whose mechanism of action (MOA) is yet to be characterized, and to investigate whether this molecule works through PPARγ, we conducted western blot on healthy and AML BM-MSC lines treated with Isoginkgetin, and then comparing the relative PPARγ expression in these cells to those treated with known PPARγ agonists such as GW1929 and Troglitazone (Fig. 3.12 a, b). (Fig. 3.12c). The expression of PPARγ did not seem to be particularly different relative to the empty control in cells treated with PPARγ-agonists (Fig. 3.12c), which indicates that during the process of adipogenic differentiation, there exists some basal expression of PPARγ. We then performed ELISA to measure the activation of PPARγ in these cells, keeping the same conditions as our western blot experiment. Activation of PPARγ can be quantified by measuring the amount of phosphorylated PPARγ in the nuclei, and in healthy BM-MSCs, treatment with PPARγ agonists such as GW1929 and Troglitazone resulted in high level of PPARγ activation compared to the empty/non-treated control, while Isoginkgetin showed no particular difference from the control (Fig. 3.12d), indicating little to no PPARγ activation. Interestingly, in AML BM-MSCs, there did not appear to be any particular difference either in the activation level of PPARγ-agonist treated conditions compared to the control (Fig. 3.12d), which suggests that PPARγ might be impaired in some manner in AML.

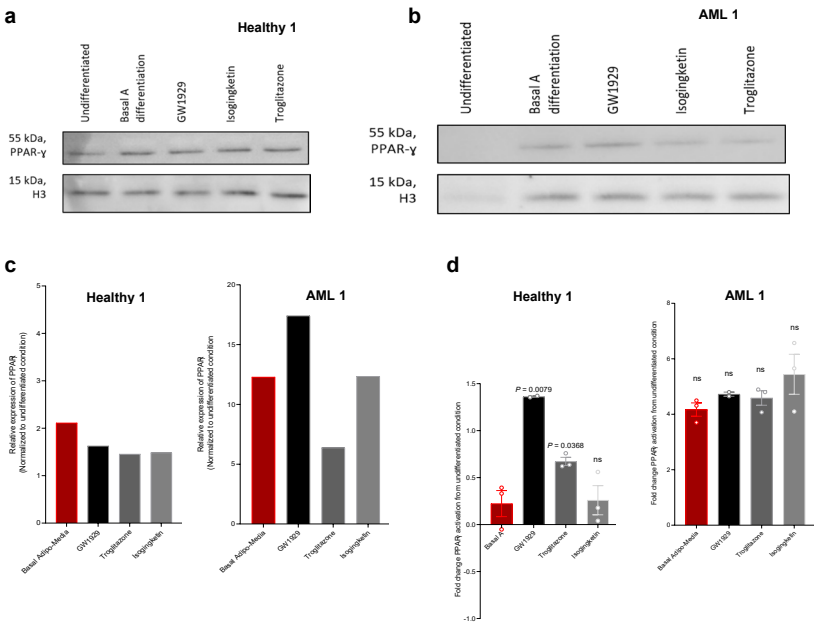

Figure 3.12: Isoginkgetin induces adipogenesis independently of PPARγ activation. (**a**, **b**) Western blot confirming the presence of PPARγ and (**c**) their relative expression in healthy (Healthy 1, left) and AML (AML 1, right) BM-MSCs when treated with Isoginkgetin in comparison to undifferentiated, empty control, or PPARγ agonists. (**d**) Activated PPARγ in the nuclei of healthy (Healthy 1, left) and AML (AML 1, right) BM-MSCs as measured through ELISA (*n*=3 technical replicates/condition). All data are shown as bars (**c**) or means ± s.e.m (**i**, **j**). Statistical analysis was assessed by unpaired *t*-test (**d**).

In conclusion, we performed a high-throughput chemical screen of compounds from the Spectrum Library and discovered a novel PPARγ-independent molecule, Isoginkgetin, that promoted adipogenic differentiation of BM-MSCs.

3.6 Isoginkgetin rescues the adipogenesis potential of mesenchymal progenitors *in vitro* and promotes adipogenesis in BM of healthy mice

3.6.1 Isoginkgetin restores the adipogenesis capacity of mesenchymal progenitors with impaired differentiation potential

We wanted to determine whether the molecule we have discovered from our BM mesenchymal *in vitro* screen can alter the differentiation capacity of mesenchymal cells at the

progenitor level. To do this, we conducted mesenchymal CFU assay on 1 healthy and 1 AML BM-MSC sample and observed their mesenchymal progenitor output upon treatment of Isoginkgetin. Consistent with our *in vitro* screen, we observed a modest increase in the adipogenesis activity of BM-MSCs in both healthy and diseased individuals, as shown by the increased proportion of all adipocyte compartments, although not to a significant extent on AML BM-MSCs (Supplementary Fig. 3.20).

To further investigate the adipogenesis-potentiating capacity of Isoginkgetin, we tested its efficacy on mesenchymal cells which had acquired impaired adipogenic differentiation potential following exposure to a leukemic environment. Repeating the conditions of our previous co-culture experiment, we supplied the differentiation media with Isoginkgetin while healthy mesenchymal colonies were exposed to the presence of leukemic blasts (Fig. 3.13a). Upon the addition of adipogenesis-inducing molecules GW1929 and Isoginkgetin, we saw an increase in both the number and proportion of adipocyte-osteoblast and adipocyte progenitors (Fig. 3.13b, c, d), although the increase in proportion of adipocyte-osteoblast progenitors did not appear to be of statistical significance for Isoginkgetin (Fig. 3.13d). Additionally, GW1929 seemed to bring the proportion of undifferentiated mesenchymal progenitors down, although again not to a significant extent, while Isoginkgetin did not appear to have an effect on the proportion of CFU-Us (Fig. 3.13d). Both GW1929 and Isoginkgetin however did increase the overall adipogenesis potential of healthy mesenchymal cells whose adipogenesis potential have been dampened by the leukemia (Fig. 3.13d, e), although for Isoginkgetin, not to the extent where it compromised the osteoblast potential of BM-MSCs as it did with GW1929 (Fig. 3.13d, e).

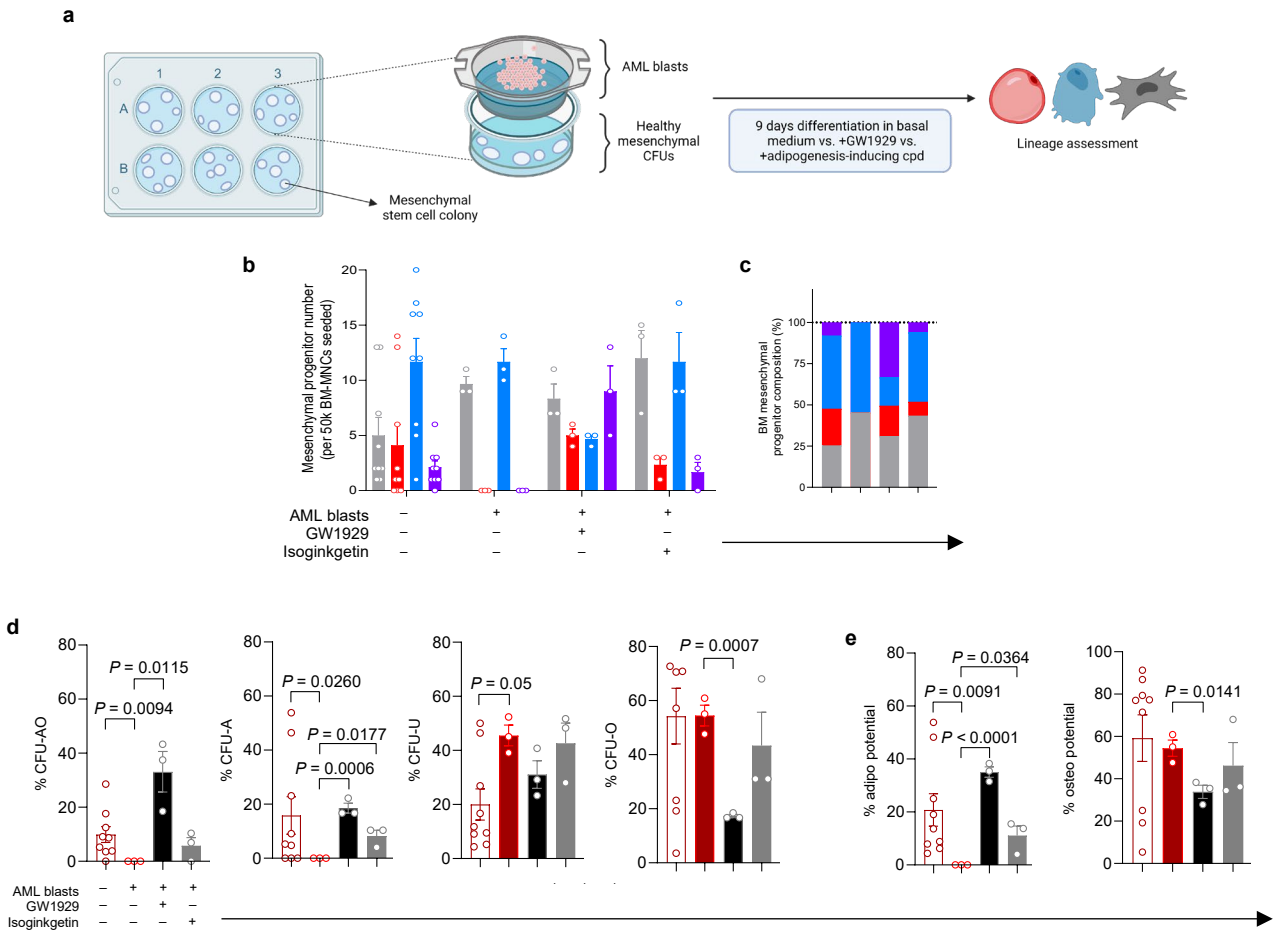

Figure 3.13: Isoginkgetin rescues adipogenesis potential of mesenchymal progenitors *in vitro*. (**a**) Schematic of experiment. Upon introduction of leukemic blasts (AML 21) in the upper Transwell chamber, differentiation media alone or media treated with adipogenesis-inducing compounds were added to the lower chamber for 9 days. (**b**) Progenitor number and (**c**) composition of healthy BM-MSCs during various co-culture conditions. *n*=9 technical replicates for the no-culture condition, *n*=3 technical replicates for all co-culture conditions (no addition of adipogenesis-inducing molecules, GW1929, and Isoginkgetin). (**d**) Proportion each mesenchymal progenitor compartment and (**e**) overall adipogenesis and osteoblastogenesis potential of healthy BM-MSCs (Healthy 2) in various co-culture conditions. For each culture condition, from left to right *n*=9, *n*=3, *n*=3, *n*=3 technical replicates per condition respectively. All data are means ± s.e.m (**b**, **c**, **d**, **e**). Statistical significance was assessed by unpaired *t*-test (**d**, **e**).

3.6.2 In vitro *administration of Isoginkgetin corrects mesenchymal progenitor composition of relapsed AML patients to resemble those of patients in remission*

Previously, we observed impaired adipogenesis potential and a heightened osteoblastic activity in mesenchymal cells from relapsed AML patients (Fig. 3.7). To determine whether Isoginkgetin can likewise reverse this increased osteoblast potential and rescue the adipogenesis capacity of MSCs from these patients, we performed mesenchymal CFU assay on one of the relapse samples that has previously shown a particularly high osteoblast potential and exposed the culture to Isoginkgetin throughout the differentiation process.

Addition of both adipogenesis-promoting molecules GW1929 and Isoginkgetin successfully increased the number and proportion of adipocyte progenitors observed (Fig. 3.14a, b, d), which in turn rescued the overall adipogenesis capacity while bringing the osteoblast potential of the sample down (Fig. 3.13c), reshaping the mesenchymal landscape into one that resembles those of patients in remission (Fig. 3.7).

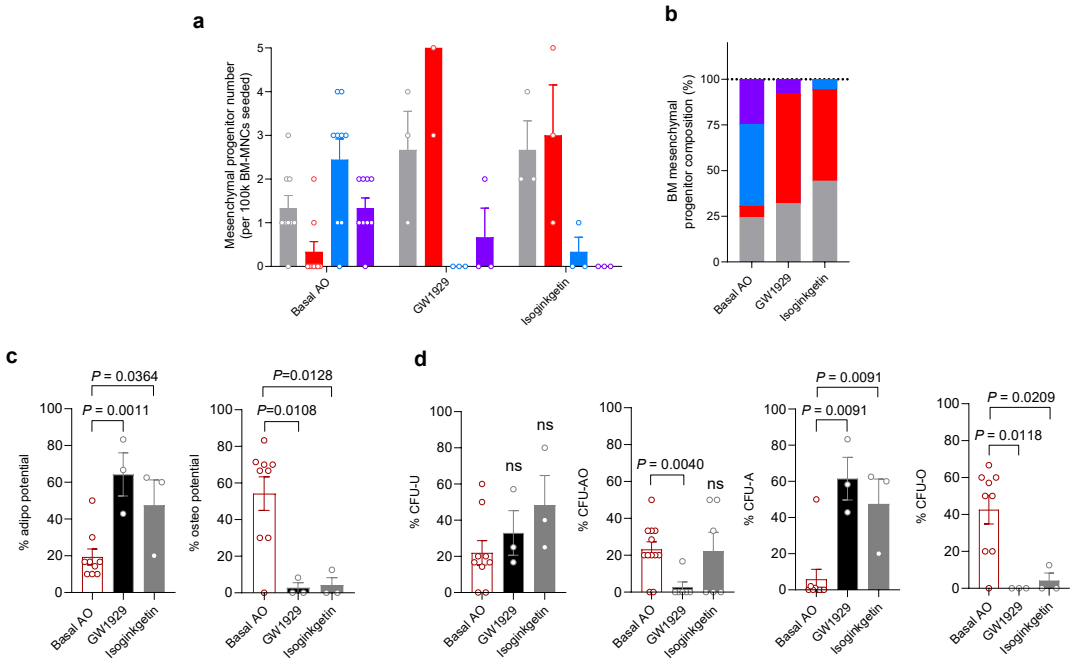

Figure 3.14: Isoginkgetin recovers the attenuated adipogenesis capacity seen upon disease regeneration. (**a**) Mean progenitor number, (**b**) composition of mesenchymal progenitors, (**c**) overall adipogenesis (left) and osteoblastogenesis (right) potential, and (**d**) proportion of each mesenchymal progenitor compartment in relapsed AML patient (AML 24.3) upon treatment of adipogenesis-inducing molecules. *n*=9 technical replicates for basal AO condition, *n*=3 technical replicates for GW1929 and Isoginkgetin conditions. All data are means ± s.e.m (**a**, **c**, **d**) or stacked means (**b**). Statistical significance was assessed by unpaired *t*-test (**c**, **d**).

3.6.3 Isoginkgetin increases BM adipocyte content of healthy mice

To test its adipogenesis-promoting capacity *in vivo*, we administered Isoginkgetin to healthy mice through oral gavage and observed the BM adipocyte content following 30 days of treatment (Fig. 3.15a). The H&E images of femurs from the Isoginkgetin and GW1929-treated groups seemed to show higher amount of adipocytes in the BM compared to those of the vehicle control group (Fig. 3.15b). Upon further immunostaining of these femurs with Perilipin, and using a quantitation pipeline which has been described in our previous study (Fig. 3.15c; Boyd et al., 2017), we found that our dosing regimen of Isoginkgetin successfully increased the frequency of adipocytes in the marrow alongside our GW1929 positive control group (Fig. 3.15d, e). Interestingly, the level at which Isoginkgetin induced adipogenesis also mirrored our *in vitro*

observation, indicating the consistency of our assays. Altogether, these *in vitro* and pre-clinical observations suggests that Isoginkgetin might be a promising pharmacological means to modulate the AML adipocytic niche.

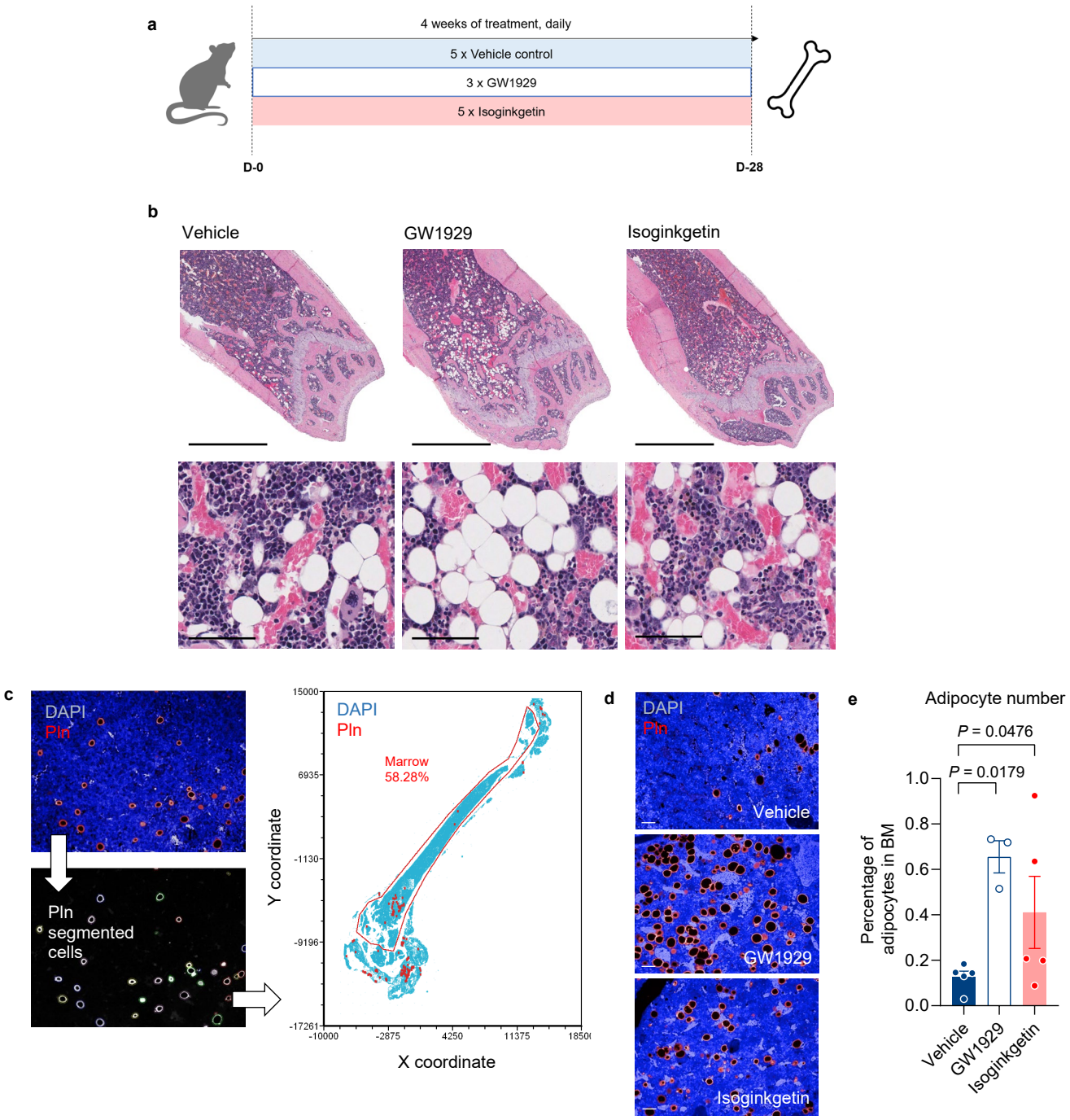

Figure 3.15: Isoginkgetin induces adipogenesis in BM of healthy mice. (**a**) Experimental design. Healthy mice were treated by oral gavage daily for 4 weeks with 20 mg/kg Isoginkgetin, 10mg/kg GW1929, or 10% DMSO in corn oil (vehicle control). (**b**) Representative images of H&E-stained mouse femurs from each treated group. Scale bars, 1000 and 60 μm for upper and lower rows, respectively. (**c**) Perilipin (Pln) staining (top left) and quantification of adipocytes (bottom left) using customized image analysis script. Different-coloured circles represent separate adipocytes and tissue was mapped onto an X-Y coordinates (right). Red line shows gating of marrow to exclude non-marrow adipocytes. (**d**) Immunofluorescent images of mice femur stained with Pln and DAPI. Scale bar, 50 μm. (**e**) Frequency of adipocytes in the bone marrow for each treated group. All data are means ± s.e.m (**e**). Statistical significance was assessed by one-tailed Mann-Whitney *U*-test (**e**).

4.0 Discussion and Conclusion

Hematopoietic cells rely on interaction with their niche in order to function properly. In many hematological malignancies such as AML, manifestation of the disease is usually accompanied by some aberration to the niche. Mesenchymal stem cells too are one of the many components of this niche; however, reports on how each mesenchymal lineage is implicated in AML often differ and contradict one another. Many observe an enhanced propensity of BM-MSCs derived from AML patients to differentiate towards the adipogenic lineage (Azadniv et al. 2019a; Le et al. 2016), but various reports showing the opposite too exist, that AML BM-MSCs are geared towards osteoblast differentiation and are in fact impaired in their adipogenesis capacity (Battula et al. 2017; Schepers et al. 2013). Indeed, studies on mesenchymal populations are challenging as they often require to be isolated and further expanded *in vitro*, which subject them to a multitude of confounding factors that can lead to biased interpretation at time of analysis.

We have shown that MSCs are plastic and exhibit promiscuity towards other lineages while they are propagated in culture, giving rise to a collection of heterogeneous population with a substantially different mesenchymal differentiation capacity compared to their initial potential at

time of plating (Fig. 3.2). Serial passaging exerts selective pressures during *in vitro* culturing of mesenchymal populations, resulting in certain subpopulations that are conditionally more competent being disproportionally expanded in a Darwinian mechanism (Fig. 3.3). Whichever subset of cells from the original population that survive and have gained the ability to adapt to the culturing condition will then make up the majority of population seen *in vitro* at time of analysis, which could contribute to the discrepancies currently observed in the field. Of course, this artifact of culture that we are observing may be further compounded by the limited amount of samples that can be tested at a time. Our study shows heterogeneity in mesenchymal differentiation capacity even amongst healthy donors (Fig. 3.2), which makes investigation of AML mesenchymal cells all the more challenging. In contrast, our approach of measuring mesenchymal differentiation capacity through the CFU assay bypasses this disproportionate selection in culture as we proceed with evaluating progenitor composition and differentiation soon following the derivation process. This method allows us to interrogate the potential of mesenchymal cells, which is not possible to do in a dynamic niche environment, and then relate back our biological observations to the pathology of the disease, making it a particularly powerful tool for studying mesenchymal populations especially in a heterogeneous malignant state such as AML.

Through our mesenchymal CFU assay, we found that at diagnosis, AML patients not only exhibit depletion of both adipocyte and osteoblast progenitors (Fig. 3.5), but they also show an increased proportion of a certain population which we define as undifferentiated mesenchymal progenitors. This entity, termed CFU-Us, lack the differentiation capacity to form both adipocytes and osteoblasts and are impaired in their proliferative ability (Fig. 3.3-3.5). While our finding complements a previous report, wherein scRNAseq of murine stromal populations during states

of homeostasis and AML reveals that MSCs in AML condition are impaired in both their adipocytic and osteoblastic capacities and acquire an undifferentiated cell state (Baryawno et al. 2019), it is the first within the mesenchymal field to functionally identify the existence of such population at the progenitor level.

To date, BMT remains the only curative treatment for AML. However, early induction mortality prior to BMT still pose as a major challenge that elderly patients need to overcome. BMT is also associated with significant morbidity and transplant-related mortality, thus prolonging patient survival becomes as important a goal as eliminating the disease. Many treatments in recent years have been developed with the goal of directly targeting leukemic cells in mind, yet still failing to address the damages incurred by the niche as a result of both the disease and the abrasive therapy regimens given to patients. Our experimental observation regarding the enrichment of undifferentiation mesenchymal populations in AML patients points to this impaired state of the niche, which manifests in patients as various forms of comorbidities, leading to their succumbing to illness despite having supposedly rid of the disease following therapies. It would be pertinent then that we elucidate the molecular profile of these undifferentiated entities and identify potential markers to be targeted.

The adipocytic niche becomes another subject of interest, as it appears to be the mesenchymal lineage that is consistently impaired in AML throughout the progression of the disease. Tracking the mesenchymal progenitor of patients who managed to achieve remission compared to those who eventually relapsed, we found that relapsed AML patients show lower adipocyte progenitors and increased osteoprogenitor activity (Fig. 3.7). As yet, we do not know

whether this remodeling of the niche stems directly from the onset of leukemia regeneration. Among the 3 BM mesenchymal lineages, adipocytes are commonly deemed as the biggest culprit in disease propagation, pointing to their role in fatty acid release which are thought to help fuel leukemic blasts (Azadniv et al. 2019a; Bijender Kumar et al. 2018; Le et al. 2016; Shafat et al. 2017; Tabe, Konopleva, and Andreeff 2020). However, emerging studies have shown that BM adipocytes represent a unique subset of adipose tissue and have distinct genetic, metabolic, and lipidomic profiles from that of white adipose tissues (Horowitz et al. 2017; Attané et al. 2020). While they may be similar morphologically, BM adipocytes are poised towards a cholesterol metabolism and in fact show an attenuated lipolysis activity (Attané et al. 2020). In addition, adipocytes derived from BM-MSCs *in vitro* are not equal functionally to BM adipocytes found *in situ* (Attané et al. 2020), as these *in vitro*-derived adipocytes show metabolic profiles of canonical white adipocytes instead. Herein, we once again reiterated the limitation of current *in vitro* assays in elucidating the function of mesenchymal populations, including adipocytes, and their tendency to fall prey to observer effects. In reality, BM adipocytes bear a much more complex role beyond their function to store lipids and posing as empty spaces within the marrow.

Addressing the injury we observed on the adipocytic niche, we discovered a novel PPARɤ-independent molecule, Isoginkgetin, which shows promising adipogenesis-initiating capacity both *in vitro* and *in vivo*. We propose the development of Isoginkgetin as an adjuvant to existing treatments, in the hopes that by recovering the adipocyte landscape, which we have shown previously to support healthy myelo-erythropoiesis during an AML diseased state (Boyd et al., 2017), we can prolong survival of patients and perhaps confer patients additional protection from

disease relapse, after recovering their mesenchymal architecture to resemble those of patients in remission (Fig. 3.14).

The future of AML studies can no longer be separated from the study of the BM microenvironment. On top of more targeted therapies, the current management of AML disease must likewise address the deficiencies in the niche such that elderly patients can be better prepared for demanding therapeutic regimens, leading to an improved survival outcome prior to and following stem cell transplantation.

Supplementary Figures

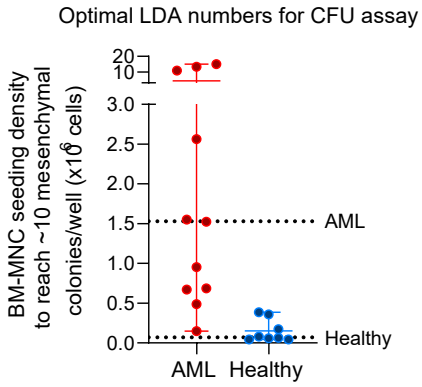

Supplementary Figure 3.16: Optimization of BM-MNCs seeding density for mesenchymal CFU assay. Range of BM-MNCs seeding density required for AML and healthy samples to reach viable counts within a well (*N*=11 independent samples for AML, *N*=8 independent samples for Healthy). Dotted lines represent median for each group. Data are shown as dot-plot.

a

Basal media	DMEM + 2% FBS	DMEM + 2% FBS	DMEM + 2% FBS	DMEM + 2% FBS	DMEM + 2% FBS	DMEM + 2% FBS	DMEM + 2% FBS	DMEM + 2% FBS	DMEM + 2% FBS	DMEM + 2% FBS
IBMX	-	-	500 uM	500 uM	500 uM	500 uM	500 uM	500 uM	500 uM	500 uM
Dexamethasone	-	-	1 uM	1 uM	1 uM	1 uM	0.1 uM	0.1 uM	-	-
Insulin	-	-	5 ug/mL	5 ug/mL	5 ug/mL	5 ug/mL	5 ug/mL	5 ug/mL	5 ug/mL	5 ug/mL
Indomethacin	-	-	50 uM	50 uM	-	-	-	-	-	-
GW1929	-	10 uM	-	10 uM	-	10 uM	-	10 uM	-	10 uM

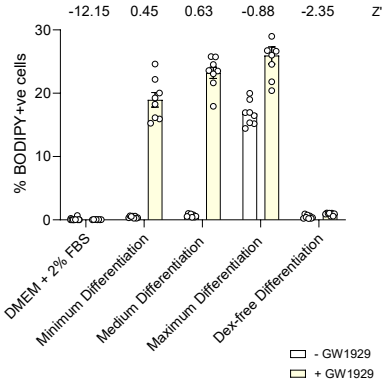

c

	Adipogenesis	Osteogenesis	Adipo-osteo	
Basal media	DMEM + 10% FBS	DMEM + 10% FBS	DMEM + 10% FBS	DMEM + 10% FBS
IBMX	500 uM	-	500 uM	500 uM
Insulin	5 ug/mL	-	5 ug/mL	5 ug/mL
Dex	1 uM	1 uM	1 uM	1 uM
Ascorbic acid 2-phosphate	-	0.2 mM	0.2 mM	0.2 mM
Glycerol 2-phosphate	-	10 mM	10 mM	10 mM
L-glut	-	1X	1X	1X
GW	-	-	-	10 uM

d

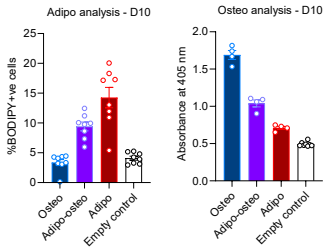

Supplementary Figure 3.17: Optimization of basal adipocyte-osteoblast differentiation medium. (**a**) Titration of reagents required for minimal induction of adipogenesis. (**b**) Sensitivity of each adipogenesis differentiation cocktail upon addition of an adipogenesis-promoting molecule i.e. induction of adipogenesis. *n*=8 technical replicates for each differentiation medium condition. (**c**) Media composition allowing for basal differentiation into adipocytes, osteoblast, or both the adipocytic and osteoblastic lineages. (**d**) Percentage of differentiated adipocytes (left) and measure of osteoblastogenesis through Alizarin red activity (right) in culture for each basal differentiation condition at day 10. *n*=8 technical replicates for each medium condition when assessing adipogenesis; *n*=4 for assessment of osteoblastogenesis. Data are shown as means ± s.e.m (**b**, **d**). Statistical significance was assessed by unpaired *t*-test (**d**).

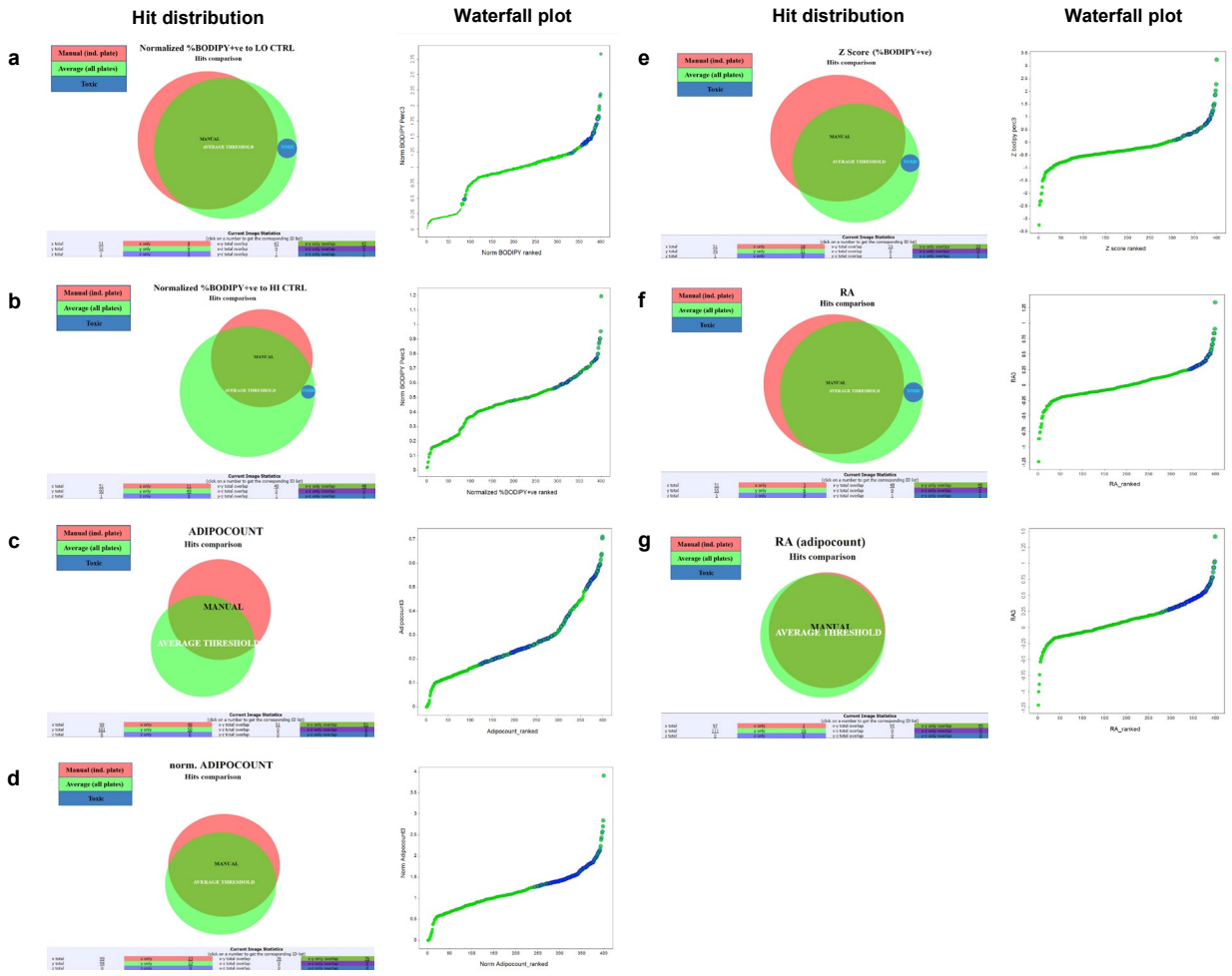

Supplementary Figure 3.18: Comparison of 7 adipogenesis outputs revealed relative activity (RA) as measured by %BODIPY+ve cells to be the best output for mining primary screen results. A total of 7 outputs were considered for analysis of data from the primary screen: (**a**) Percentage of BODIPY+ve cells normalized to low DMSO control. (**b**) Percentage of BODIPY+ve cells normalized to high GW1929 control. (**c**) The product of normalized cell count and percentage BODIPY+ve cells (denoted as adipocount). (**d**) Adipocount normalized to low DMSO control. (**e**) Z score as measured by percentage of BODIPY+ve cells. (**f**) Relative activity (RA) measuring percentage of BODIPY+ve cells, and lastly. (**g**) RA measuring adipocount. For venn diagrams coloured in pink, hit calculations were performed individually for each plate, whereas venn diagrams in green showed population of hits obtained using a calculated threshold of all the plates. Dots highlighted in blue on the waterfall plots corresponded to hit populations determined after calculation for each individual plate. RA (% BODIPY+ve) seemed to give the best readout that encompassed most of the hit populations, as well as a good distribution on the waterfall plot.

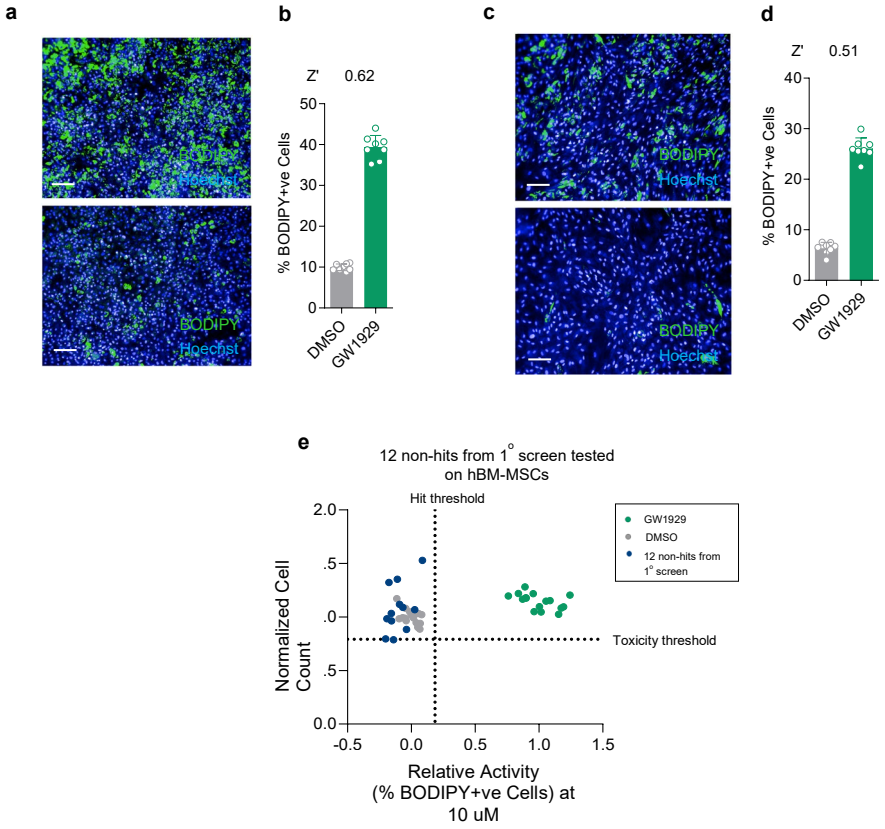

Supplementary Figure 3.19: Robustness and sensitivity of adipogenesis screen on BM-MSCs. (**a**) Representative fluorescent images of iMSC3s treated with GW1929 positive control (top) and 0.1% DMSO (bottom). Green denotes BODIPY staining while live cells are shown through Hoechst staining in blue. Scale bars, 300 µm. (**b**) Sensitivity of primary screen on iMSC3 measured through Z score. (**c**) Representative fluorescent images of positive (top) and empty (bottom) controls for secondary screen on primary BM-MSCs (Healthy 13). Scale bars, 300 µm. (**d**) Sensitivity of secondary screen as measured through Z score. (**e**) Validation of primary screen. 12 random non-hits (grey) from the primary screen were tested on Healthy 13 (BM-MSC line used in secondary screen). Blue dots (*n*=12) represent empty controls while green dots denote positive controls (*n*=12). Data are shown as means ± s.e.m (**b**, **d**) or dot plot (**e**).

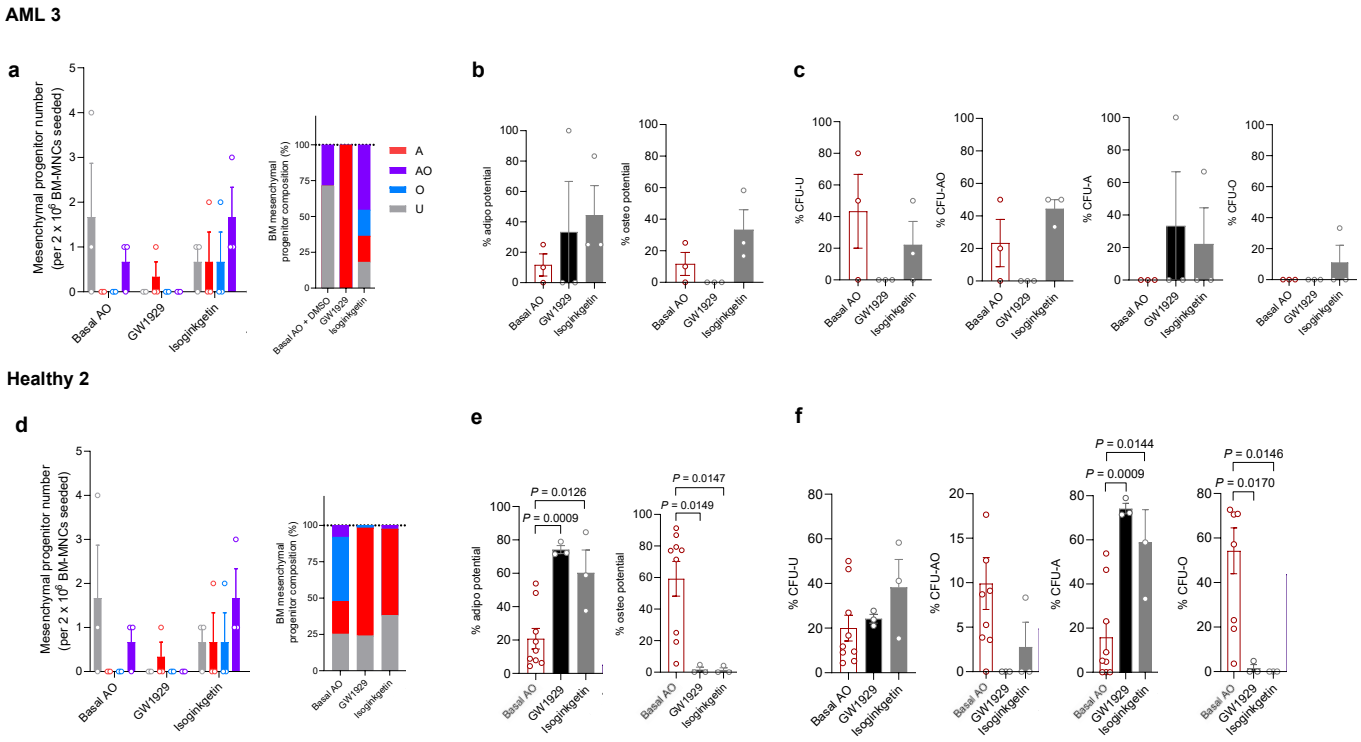

Supplementary Figure 3.20: Isoginkgetin increases adipogenesis potential of AML and healthy BM-MSCs. (**a**) Mesenchymal progenitor number (left) and composition (right), (**b**) adipogenesis (left) and osteoblastogenesis (right) potential, and (**c**) proportion of each mesenchymal progenitor compartment of AML BM-MSCs (AML 3) following treatment with adipogenesis-inducing molecules. *n*=3 technical replicates for each condition. (**d**) Progenitor number (left) and composition (right), (**e**) overall adipogenesis and osteoblastogenesis potential, and (**f**) percentage of each mesenchymal progenitor type within BM-MSCs from a healthy donor (Healthy 2) following treatment with adipogenesis-inducing molecules. *n*=9 technical replicates for basal differentiation control, *n*=3 technical replicates for GW1929 and Isoginkgetin conditions. Data are shown as means ± s.e.m (**a**, **d**, left; **b**, **c**, **e**, **f**) or stacked means (**a**, **d**, right). Statistical significance was assessed by unpaired *t*-test (**b**, **c**, **e**, **f**).

5.0 Bibliography

Abdul-aziz, Amina M et al. 2019. "Acute Myeloid Leukemia Induces Protumoral P16INK4a-Driven Senescence in the Bone Marrow Microenvironment." *Blood* 133(5): 446–56.

Abramson, Sydney, Richard G. Miller, and Robert A. Phillips. 1977. "The Identification in Adult Bone Marrow of Pluripotent and Restricted Stem Cells of the Myeloid and Lymphoid Systems*." *Journal of Experimental Medicine* 145(6): 1567–79.

Ambrosi, Thomas H. et al. 2017. "Adipocyte Accumulation in the Bone Marrow during Obesity and Aging Impairs Stem Cell-Based Hematopoietic and Bone Regeneration." *Cell Stem Cell* 20(6): 771-784.e6.

Arber, Daniel A. et al. 2016. "The 2016 Revision to the World Health Organization Classification of Myeloid Neoplasms and Acute Leukemia." *Blood* 127(20): 2391–2405.

Attané, Camille et al. 2020. "Human Bone Marrow Is Comprised of Adipocytes with Specific Lipid Metabolism." *Cell Reports* 30(4): 949-958.e6.

Azadniv, Mitra et al. 2019a. "Bone Marrow Mesenchymal Stromal Cells from Acute Myelogenous Leukemia Patients Demonstrate Adipogenic Differentiation Propensity with Implications for Leukemia Cell Support." *Leukemia* 34: 391–403. http://dx.doi.org/10.1038/s41375-019-0568-8.

———. 2019b. "Bone Marrow Mesenchymal Stromal Cells from Acute Myelogenous Leukemia Patients Demonstrate Adipogenic Differentiation Propensity with Implications for Leukemia Cell Support."

Baryawno, Ninib et al. 2019. "A Cellular Taxonomy of the Bone Marrow Stroma in Homeostasis and Leukemia." *Cell* 177: 1–18. https://doi.org/10.1016/j.cell.2019.04.040.

Battula, V Lokesh et al. 2017. "AML-Induced Osteogenic Differentiation in Mesenchymal Stromal Cells Supports Leukemia Growth." *JCI Insight* 2(13): e90036.

Bejanyan, Nelli et al. 2015. "Survival of Patients with Acute Myeloid Leukemia Relapsing after Allogeneic Hematopoietic Cell Transplantation: A Center for International Blood and Marrow Transplant Research Study." *Biology of Blood and Marrow Transplantation* 21(3): 454–59. http://dx.doi.org/10.1016/j.bbmt.2014.11.007.

Bianco, Paolo et al. 2013. "The Meaning, the Sense and the Significance: Translating the Science of Mesenchymal Stem Cells into Medicine." *Nature Medicine* 19(1): 35–42.

Bianco, Paolo, Pamela Gehron Robey, and Paul J Simmons. 2008. "Mesenchymal Stem Cells: Revisiting History, Concepts, and Assays." *Cell Stem Cell* 2: 313–19.

Bock, Thomas A. 1997. "Assay Systems for Hematopoietic Stem and Progenitor Cells." *Stem Cells* 15(S2): 185–95. https://academic.oup.com/stmcls/article/15/S2/185/6391043 (June 19, 2022).

Bonab, Mandana Mohyeddin et al. 2006. "Aging of Mesenchymal Stem Cell in Vitro." *BMC Cell Biology* 7(14): 1–7.

Bonnet, Dominique, and John E Dick. 1997. "Human Acute Myleoid Leukemia Is Organized as a Hierarchy That Originates from a Primitive Hematopoietic Cell." *Nature Medicine* 3(7): 730–37.

Boyd, Allison L et al. 2014. "Niche Displacement of Human Leukemic Stem Cells Uniquely Allows Their Competitive Replacement with Healthy HSPCs." *Journal of Experimental Medicine* 211(10): 1925–35.

———. 2017. "Acute Myeloid Leukaemia Disrupts Endogenous Myelo-Erythropoiesis by Compromising the Adipocyte Bone Marrow Niche." *Nature Cell Biology* 19(11): 1336–47.

———. 2018. “Identification of Chemotherapy-Induced Leukemic- Regenerating Cells Reveals a Transient Vulnerability of Human AML Recurrence.” *Cancer Cell* 34(3): 483–98. https://doi.org/10.1016/j.ccell.2018.08.007.

Clarke, E, and S R McCann. 1989. “Age Dependent in Vitro Stromal Growth.” *Bone Marrow Transplantation* 4(5): 596–97.

Daver, Naval G. et al. 2019. “Azacitidine (AZA) with Nivolumab (Nivo), and AZA with Nivo + Ipilimumab (Ipi) in Relapsed/Refractory Acute Myeloid Leukemia: A Non-Randomized, Prospective, Phase 2 Study.” *Blood* 134(Supplement_1): 830–830. http://dx.doi.org/10.1182/blood-2019-131494.

Dick, John E. et al. 1997. “Assay of Human Stem Cells by Repopulation of NOD/SCID Mice.” *Stem Cells* 15(SUPPL. 1): 199–207.

Dominici, M et al. 2006. “Minimal Criteria for Defining Multipotent Mesenchymal Stromal Cells. The International Society for Cellular Therapy Position Statement.” *Cytotherapy* 8(4): 315–17. http://dx.doi.org/10.1080/14653240600855905.

Estey, Elihu H. 2020. “Acute Myeloid Leukemia: 2021 Update on Risk-Stratification and Management.” *American Journal of Hematology* 95(11): 1368–98.

Farmer, Stephen R. 2006. “Transcriptional Control of Adipocyte Formation.” *Cell Metabolism* 4(October): 263–73.

Friedenstein, A. J. 1980. “Stromal Mechanisms of Bone Marrow: Cloning in Vitro and Retransplantation in Vivo.” *Haematology and blood transfusion* 25: 19–29. https://pubmed.ncbi.nlm.nih.gov/7021339/ (March 11, 2021).

Friedenstein, A. J., R. K. Chailakhjan, and K. S. Lalykina. 1970. “The Development of Fibroblast Colonies in Monolayer Cultures of Guinea-Pig Bone Marrow and Spleen Cells.” *Cell Proliferation* 3(4): 393–403. https://pubmed.ncbi.nlm.nih.gov/5523063/ (March 11, 2021).

Friedenstein, A. J., R. K. Chailakhyan, and U. V. Gerasimov. 1987. “Bone Marrow Osteogenic Stem Cells: In Vitro Cultivation and Transplantation in Diffusion Chambers.” *Cell Proliferation* 20(3): 263–72. https://pubmed.ncbi.nlm.nih.gov/3690622/ (March 11, 2021).

Friedenstein, A J, K V Petrakova, A I Kurolesova, and G P Frolova. 1968. “Heterotopic of Bone Marrow. Analysis of Precursor Cells for Osteogenic and Hematopoietic Tissues.” *Transplantation* 6(2): 230–47.

Friedenstein, A J, I Piatetzky-Shapiro, and & K V Petrakova. 1966. 16 Embryol. exp. Morph *Osteogenesis in Transplants of Bone Marrow Cells*.

Friedenstein, Alexander J. et al. 1974. “Stromal Cells Responsible for Transferring the Microenvironment of the Hemopoietic Tissues: Cloning in Vitro and Retransplantation in Vivo.” *Transplantation* 17(4): 331–40.

Frisch, Benjamin J et al. 2012. “Functional Inhibition of Osteoblastic Cells in an in Vivo Mouse Model of Myeloid Leukemia.” *Blood* 119(2): 540–50.

Ganguly, Payal et al. 2017. “Age-Related Changes in Bone Marrow Mesenchymal Stromal Cells: A Potential Impact on Osteoporosis and Osteoarthritis Development.” *Cell Transplantation* 26(9): 1520–29.

Goodell, Margaret A, Hoang Nguyen, and Noah Shroyer. 2015. “Somatic Stem Cell Heterogeneity: Diversity in the Blood, Skin and Intestinal Stem Cell Compartments.” *Nature Reviews Molecular Cell Biology* 16: 299–309.

Hanoun, Maher et al. 2014. “Acute Myelogenous Leukemia-Induced Sympathetic Neuropathy Promotes Malignancy in an Altered Hematopoietic Stem Cell Niche.” *Cell Stem Cell* 15:

365–75.
Hardouin, Pierre, Tareck Rharass, and Stéphanie Lucas. 2016. "Bone Marrow Adipose Tissue: To Be or Not To Be a Typical Adipose Tissue?" *Frontiers in Endocrinology* 7(June): 1–11.
Home, Philip. 2011. "Safety of PPAR Agonists." *Diabetes Care* 34.
Hope, Kristin J., Liqing Jin, and John E. Dick. 2004. "Acute Myeloid Leukemia Originates from a Hierarchy of Leukemic Stem Cell Classes That Differ in Self-Renewal Capacity." *Nature Immunology* 5(7): 738–43.
Horowitz, Mark C et al. 2017. "Bone Marrow Adipocytes." *Adipocyte* 6(3): 193–204.
Imai, Takeshi et al. 2004. "Peroxisome Proliferator-Activated Receptor γ Is Required in Mature White and Brown Adipocytes for Their Survival in the Mouse." *PNAS* 101(13): 4543–47.
Jaiswal, Siddhartha et al. 2009. "CD47 Is Upregulated on Circulating Hematopoietic Stem Cells and Leukemia Cells to Avoid Phagocytosis." *Cell* 138(2): 271–85. http://dx.doi.org/10.1016/j.cell.2009.05.046.
José Albuquerque de Paula, Francisco, and Clifford J. Rosen. 2018. "Structure and Function of Bone Marrow Adipocytes." *Comprehensive Physiology* 8(January): 315–49.
Ka, Li et al. 2014. "The Surface Markers and Identity of Human Mesenchymal Stem Cells." *Stem Cells* 32: 1408–19.
Kouchkovsky, I De, and M Abdul-Hay. 2016. "'Acute Myeloid Leukemia: A Comprehensive Review and 2016 Update.'" *Blood Cancer Journal* 6: e441.
Krevvata, Maria et al. 2014. "Inhibition of Leukemia Cell Engraftment and Disease Progression in Mice by Osteoblasts." *Blood* 124(18): 2834–46.
Kronstein-Wiedemann, Romy, and Torsten Tonn. 2019. "Colony Formation: An Assay of Hematopoietic Progenitor Cells." In *Stem Cell Mobilization*, eds. Gerd Klein and Patrick Wuchter. New York, NY: Springer New York, 29–40. https://doi.org/10.1007/978-1-4939-9574-5_3,.
Kumar, B et al. 2018. "Acute Myeloid Leukemia Transforms the Bone Marrow Niche into a Leukemia-Permissive Microenvironment through Exosome Secretion." *Leukemia* 32: 575–87.
Kumar, Bijender et al. 2018. "Leukemia Cells Remodel Adipocyte Niches and Their Progenitor Functions to Generate Leukemia Favoring Niche." *Blood* 132(Supplement 1): 1294–1294. http://dx.doi.org/10.1182/blood-2018-99-115689.
Lapidot, Tsvee et al. 1994. "A Cell Initiating Human Acute Myeloid Leukaemia after Transplantation into SCID Mice." *Nature* 367: 645–48.
Le, Yevgeniya et al. 2016. "Adipogenic Mesenchymal Stromal Cells from Bone Marrow and Their Hematopoietic Supportive Role: Towards Understanding the Permissive Marrow Microenvironment in Acute Myeloid Leukemia." *Stem Cell Reviews and Reports* 12(2): 235–44.
Lefterova, Martina I, Anders K Haakonsson, Mitchell A Lazar, and Susanne Mandrup. 2014. "PPARγ and the Global Map of Adipogenesis and Beyond." *Cell* 25(6).
Lehrke, Michael, and Mitchell A Lazar. 2005. "The Many Faces of PPARγ." *Cell* 123: 993–99.
Leuven, Katholieke Universiteit. 2011. "Concise Review: Culture Mediated Changes in Fate and/or Potency of Stem Cells." *Stem Cells* 29: 583–89.
Lowell, Bradford B. 1999. "PPARγ: An Essential Regulator of Adipogenesis and Modulator of Fat Cell Function." *Cell* 99(1997): 239–42.
Majeti, Ravindra et al. 2009. "CD47 Is an Adverse Prognostic Factor and Therapeutic Antibody Target on Human Acute Myeloid Leukemia Stem Cells." *Cell* 138(2): 286–99.

http://dx.doi.org/10.1016/j.cell.2009.05.045.
Moisan, Annie et al. 2015. "White-to-Brown Metabolic Conversion of Human Adipocytes by JAK Inhibition." *Nature Cell Biology* 17(1).
Morrison, Sean J, and David T Scadden. 2014. "The Bone Marrow Niche for Haematopoietic Stem Cells." *Nature* 505(7483): 2–9.
Nakagami, Hironori. 2013. "The Mechanism of White and Brown Adipocyte Differentiation." *Diabetes & Metabolism Journal* 37: 85–90.
Naveiras, Olaia et al. 2009. "Bone-Marrow Adipocytes as Negative Regulators of the Haematopoietic Microenvironment." *Nature* 460(7252): 259–63. http://dx.doi.org/10.1038/nature08099.
Passaro, Diana et al. 2015. "CXCR4 Is Required for Leukemia-Initiating Cell Activity in T Cell Acute Lymphoblastic Leukemia." *Cancer Cell* 27(6): 769–79.
Pinho, Sandra, and Paul S Frenette. 2019. "Haematopoietic Stem Cell Activity and Interactions with the Niche." *Nature Reviews Molecular Cell Biology* 20: 303–20. http://dx.doi.org/10.1038/s41580-019-0103-9.
Pitt, Lauren A. et al. 2015. "CXCL12-Producing Vascular Endothelial Niches Control Acute T Cell Leukemia Maintenance." *Cancer Cell* 27(6): 755–68. http://dx.doi.org/10.1016/j.ccell.2015.05.002.
Pouzolles, Marie, Leal Oburoglu, Naomi Taylor, and Valérie S. Zimmermann. 2016. "Hematopoietic Stem Cell Lineage Specification." *Current Opinion in Hematology* 23(4): 311–17.
Rashidi, Armin, and John F Dipersio. 2016. "Targeting the Leukemia – Stroma Interaction in Acute Myeloid Leukemia: Rationale and Latest Evidence." *Therapeutic Advances in Hematology* 7(1): 40–51.
Rauner, Martina et al. 2016. "Increased EPO Levels Are Associated with Bone Loss in Mice Lacking PHD2 in EPO-Producing Cells." *Journal of Bone and Mineral Research* 31(10): 1877–87.
Rosen, Evan D et al. 1999. "PPARγ Is Required for the Differentiation of Adipose Tissue In Vivo and In Vitro." *Molecular Cell* 4: 611–17.
Rundberg, Alexandra, Cornelis J H Pronk, and David Bryder. 2015. "Probing Hematopoietic Stem Cell Function Using Serial Transplantation: Seeding Characteristics and the Impact of Stem Cell Purification." *Experimental Hematology* 43(9): 812-817.e1. http://dx.doi.org/10.1016/j.exphem.2015.05.003.
Schepers, Koen et al. 2013. "Myeloproliferative Neoplasia Remodels the Endosteal Bone Marrow Niche into a Self-Reinforcing Leukemic Niche." *Cell Stem Cell* 13: 285–99.
Schepers, Koen, Timothy B Campbell, and Emmanuelle Passegué. 2015. "Normal and Leukemic Stem Cell Niches: Insights and Therapeutic Opportunities." *Cell Stem Cell* 16: 254–67.
Schmid, Christoph et al. 2012. "Treatment, Risk Factors, and Outcome of Adults with Relapsed AML after Reduced Intensity Conditioning for Allogeneic Stem Cell Transplantation." *Blood* 119(6): 1599–1606.
Shafat, Manar S et al. 2017. "Leukemic Blasts Program Bone Marrow Adipocytes to Generate a Protumoral Microenvironment." *Blood* 129(10): 2–4.
Sisakhtnezhad, Sajjad, Elham Alimoradi, and Hassan Akrami. 2017. "External Factors Influencing Mesenchymal Stem Cell Fate in Vitro." *European Journal of Cell Biology* 96(1): 13–33.
Sison, Edward Allan R., and Patrick Brown. 2011. "The Bone Marrow Microenvironment and

Leukemia: Biology and Therapeutic Targeting." *Expert Review of Hematology* 4(3): 271–83.

Smith, Martyn T. 2003. "Mechanisms of Troglitazone Hepatotoxicity." *Chemical Research in Toxicology* 16(6): 679–87.

Styczyński, Jan et al. 2020. "Death after Hematopoietic Stem Cell Transplantation: Changes over Calendar Year Time, Infections and Associated Factors." *Bone Marrow Transplantation* 55(1): 126–36. https://doi.org/10.1038/s41409-019-0624-z (March 11, 2021).

Tabe, Yoko, Marina Konopleva, and Michael Andreeff. 2020. "Fatty Acid Metabolism, Bone Marrow Adipocytes, and AML." *Frontiers in Oncology* 10(February): 1–7.

Tikhonova, Anastasia N et al. 2019. "The Bone Marrow Microenvironment at Single-Cell Resolution." *Nature* 569: 222–28.

Trayhurn, Paul, and John H Beattie. 2001. "Physiological Role of Adipose Tissue: White Adipose Tissue as an Endocrine and Secretory Organ." *Proceedings of the Nutrition Society* 60: 329–39.

Tsirigotis, P et al. 2016. "Relapse of AML after Hematopoietic Stem Cell Transplantation: Methods of Monitoring and Preventive Strategies. A Review from the ALWP of the EBMT." *Bone Marrow Transplantation* 51: 1431–38.

Vardiman, James W. et al. 2009. "The 2008 Revision of the World Health Organization (WHO) Classification of Myeloid Neoplasms and Acute Leukemia: Rationale and Important Changes." *Blood* 114(5): 937–51.

Wagner, Wolfgang et al. 2008. "Replicative Senescence of Mesenchymal Stem Cells: A Continuous and Organized Process." *PLoS ONE* 3(5): e2213.

Whitfield, Matthew J, Wong Cheng, J Lee, and Krystyn J Van Vliet. 2013. "Onset of Heterogeneity in Culture-Expanded Bone Marrow Stromal Cells." *Stem Cell Research* 11(3): 1365–77. http://dx.doi.org/10.1016/j.scr.2013.09.004.

Witkowski, Matthew T, Stavroula Kousteni, and Iannis Aifantis. 2019. "Mapping and Targeting of the Leukemic Microenvironment." *Journal of Experimental Medicine* 217(2): 1–13.

Wognum, Albertus W., Allen C. Eaves, and Terry E. Thomas. 2003. "Identification and Isolation of Hematopoietic Stem Cells." *Archives of Medical Research* 34(6): 461–75.

Wolock, Samuel L et al. 2019. "Mapping Distinct Bone Marrow Niche Populations and Their Differentiation Paths." *Cell Reports* 28(2): 302–11. https://doi.org/10.1016/j.celrep.2019.06.031.

Zhou, Bo O et al. 2017. "Bone Marrow Adipocytes Promote the Regeneration of Stem Cells and Haematopoiesis by Secreting SCF." *Nature Cell Biology* 19(8): 891–903.

Zinngrebe, Julia, Klaus Michael Debatin, and Pamela Fischer-Posovszky. 2020. "Adipocytes in Hematopoiesis and Acute Leukemia: Friends, Enemies, or Innocent Bystanders?" *Leukemia* 34(9): 2305–16. http://dx.doi.org/10.1038/s41375-020-0886-x.